Metasomatism of continental crust during subduction: the UHP whiteschists from the Southern Dora-Maira Massif (Italian Western Alps)

UNIVERSITÀ DEGLI STUDI DI TORINO

Journal of METAMORPHIC GEOLOGY

Metasomatism of continental crust during subduction: The UHP whiteschists from the Southern Dora-Maira Massif (Italian Western Alps)

Journal:	*Journal of Metamorphic Geology*
Manuscript ID:	JMG-09-0030.R2
Manuscript Type:	Original Article
Date Submitted by the Author:	
Complete List of Authors:	Ferrando, Simona; University of Torino, Department of Mineralogical and Petrological Sciences Frezzotti, Maria Luce; University of Siena, Department of Earth Sciences Petrelli, Maurizio; University of Perugia, Department of Earth Sciences Compagnoni, Roberto; University of Torino, Department of Mineralogical and Petrological Sciences
Keywords:	HP metasomatic fluid, multiphase-solid inclusions, trace-element geochemistry, serpentinite, antigorite breakdown

Metasomatism of continental crust during subduction: The UHP whiteschists from the Southern Dora-Maira Massif (Italian Western Alps)

S. FERRANDO, [1] M.L. FREZZOTTI, [2] M. PETRELLI[3] AND R. COMPAGNONI[1]
[1] *Department of Mineralogical and Petrological Sciences, University of Torino, Via Valperga Caluso 35, I-10125 Torino, Italy (simona.ferrando@unito.it).*
[2] *Department of Earth Sciences, University of Siena, Via Laterina 8, I-53100 Siena, Italy.*
[3] *Department of Earth Sciences, University of Perugia, P.zza Università 1, I-06100 Perugia, Italy.*

SHORT TITLE: Continental crust metasomatism in subduction

ABSTRACT

The ultrahigh-pressure pyrope whiteschists from the Brossasco-Isasca Unit of the Southern Dora-Maria Massif represent metasomatic rocks originated at the expense of post-Variscan granitoids by the influx of fluids along shear zones. In this study, geochemical, petrological, and fluid-inclusion data, correlated with different generations of pyrope-rich garnets (from medium, to very-coarse-grained in size) allow constraints to be placed on the relative timing of metasomatism and sources of the metasomatic fluid.

Geochemical investigations reveal that whiteschists are strongly enriched in Mg and depleted in Na, K, Ca, and LILE (Cs, Pb, Rb, Sr, Ba) with respect to the metagranite. Three generations of pyrope, with different composition and mineral inclusions, have been distinguished: (1) the prograde Prp I, which constitutes the large core of megablasts and the small core of porphyroblasts; (2) the peak Prp II, which constitutes the inner rim of megablasts and porphyroblasts and the core of small neoblasts; and (3) the early retrograde Prp III, which locally constitutes an outer rim. Two generations of fluid inclusions have been recognised: (1) primary fluid inclusions in prograde kyanite that represent a NaCl-$MgCl_2$-rich brine (6–28 wt% $NaCl_{eq}$ with Si and Al as other dissolved cations) trapped during growth of Prp I (type-I fluid); (2) primary multiphase-solid inclusions in Prp II that are remnants of an alumino-silicate aqueous solution,containing Mg, Fe, alkalies, Ca and subordinate P, Cl, S, CO_3^{2-}, LILE (Pb, Cs, Sr, Rb, K, LREE, Ba), U, and Th (type-II fluid), at the peak pressure stage.

We propose a model that illustrates the prograde metasomatic and metamorphic evolution of the whiteschists and that could also explain the genesis of other Mg-rich, alkali-poor schists of the Alps. During Alpine metamorphism, the post-Variscan metagranite of the Brossasco-Isasca Unit experienced a prograde metamorphism at HP conditions (stage A: $P \sim 1.6$ GPa and $T \leq 600$ °C), as indicated by the growth of an almandine-rich garnet in some xenoliths. At stage B (1.7–2.1 GPa and 560–590 °C), the influx of external fluids, originated from antigorite breakdown in subducting oceanic serpentinites, promoted the increase in Mg and the decrease of alkalies and Ca in the orthogneiss toward a whiteschist composition. During stage C ($2.1 < P < 2.8$ GPa and $590 < T < 650$ °C), the metasomatic fluid influx coupled with internal dehydration reactions involving Mg-chlorite promoted the growth of Prp I in the presence of the type-I $MgCl_2$-brine. At the metamorphic peak (stage D: 4.0–4.3 GPa and 730 °C), Prp II growth occurred in the presence of a type–II alumino-silicate aqueous solution, mostly generated by internal dehydration reactions involving phlogopite and talc. The contribution of metasomatic external brines at the metamorphic climax appears negligible. This fluid, showing enrichment in LILE and depletion in HFSE, could represent a metasomatic agent for the supra-subduction mantle wedge.

Keywords: HP metasomatic fluid; multiphase-solid inclusions; trace-element geochemistry; serpentinite; antigorite breakdown

INTRODUCTION

Pyrope whiteschists from the Brossasco-Isasca Unit (BIU) of the Southern Dora-Maira Massif (Western Alps)—i.e., talc-phengite-kyanite-pyrope-quartz(/coesite) rocks characterised by an extremely high Mg/Fe ratio, high Si_2O, and the virtual absence of Ca and Na—became well known to the scientific community because of the first finding of coesite in crustal lithologies (i.e., the first evidence that continental crust can subduct to depths of at least 100 km; Chopin, 1984). Since this discovery, a number of studies have been carried out on Dora-Maira whiteschists to characterise the metamorphic evolution of continental crust during subduction to ultrahigh-pressure (UHP) conditions.

The composition, crystal structure, and sometimes also the stability field of major (e.g., pyrope, phengite) and minor (e.g., bearthite, ellenbergerite, Mg-dumortierite, wagnerite) minerals have been characterised (e.g., Chopin, 1986; Schertl *et al*., 1991; Chopin *et al*., 1986; 1995; Chopin & Schertl, 1999; Chopin & Ferraris, 2003 and references therein). Schertl *et al*. (1991) distinguished prograde pyrope megablasts and peak smaller pyropes. Prograde pyrope megablasts, formed at the expense of chlorite + talc + kyanite, have inclusions of kyanite, talc, chlorite, ellenbergerite, glaucophane, phlogopite (usually retrogressed to vermiculite), rutile, zircon, tourmaline, apatite, and Mg-dumortierite. Smaller peak pyrope crystals, formed at the expense of talc + kyanite, include coesite, kyanite, talc, phengite, rutile, zircon, and tourmaline.

Recent petrological and experimental studies of BIU whiteschists, in particular from the Po Valley in Italy, have constrained a *P-T* evolution characterised by six main stages: (1) a poorly constrained prograde stage at $T \leq 600$ °C and $P \sim 1.6$ GPa (Schertl *et al*., 1991; Compagnoni & Hirajima, 2001), (2) a second prograde stage at about 700–720 °C and 2.9–3 GPa (Schertl *et al*., 1991; Simon *et al*., 1997), (3) a UHP peak stage at 730 °C and 4.3 GPa, (4) an early decompression stage at 4–3.5 GPa, (5) a first decompression and cooling stage at 700–670 °C and 3–2.5 GPa, and (6) a second decompression and cooling stage at 600 °C and 1.1 GPa (Hermann, 2003). The UHP peak has been dated at about 35 Ma by U-Pb and Lu-Hf analyses on ellenbergerite, zircon, monazite, and garnet (Tilton *et al*., 1989; Duchêne *et al*., 1997; Gebauer *et al*., 1997; Vaggelli *et al*., 2006).

There is a general agreement concerning the petrology and geochronology of the Dora-Maira whiteschists, but the origin of the unusual chemical composition of these rocks is still a matter of debate. Chopin (1984) and Schertl *et al*. (1991) proposed a sedimentary protolith (a clay-evaporite composed of quartz, Mg-chlorite, and illite), whereas Compagnoni & Hirajima (1992) first proposed a metasomatic origin, suggesting a fluid influx in the metagranite along ductile shear zones during prograde UHP evolution. Stable-isotope and fluid-inclusion studies have provided further data useful for understanding the origin of whiteschists and the fluid-rock interaction processes. On the basis of stable-isotope data, Sharp *et al*. (1993) interpreted the whiteschists as metasomatic rocks that originated by the influx of metasomatic fluids from the subducting oceanic lithosphere (in addition, see Demény *et al*., 1997). They also concluded that during pyrope growth the water activity was low ($a_{H2O} = 0.4–0.75$) and that during the prograde, peak, and retrograde metamorphism X_{CO2} was low (<0.02). In pyrope megablasts from whiteschists, the fluid-inclusion study of Philippot *et al*. (1995) allowed the recognition of a prograde/peak brine consisting of magnesite, Mg-phosphate, chloride, talc or Mg-chlorite, and an opaque mineral. This brine was interpreted as a residual fluid that had remained after prograde *in-situ* generation of a melt, which should be represented by the "jadeite quartzite" closely associated with the whiteschists in the field. The presence of a melt, already suggested by Sharp *et al*. (1993) to explain the low a_{H2O} in the system, was subsequently excluded by Hermann (2003).

After the isotopic study of Tilton *et al*. (1989), which revealed that whiteschists still retain a strong crustal Pb-Nd-Sr isotope signature similar to that of granites, the metasomatic origin of the whiteschists at the expense of the hosting orthogneiss was conclusively confirmed by cathodoluminescence and SHRIMP studies on zircons (Gebauer *et al*. (1997). However, these Authors disagreed with Compagnoni & Hirajima (1992) and Sharp *et al*. (1993) about the timing of

the metasomatism (they considered it to be earlier than subduction) and the origin of the metasomatic fluid (they considered it to be derived from evaporitic metasediments).

More recently, Compagnoni & Hirajima (2001) reported superzoned garnets characterised by a reddish-brown zoned almandine core ($Alm_{70-58}Prp_{25-37}$) and a pinkish, zoned pyrope rim ($Alm_{58-14}Prp_{38-84}$) from a UHP whiteschist interpreted as a former xenolith within the orthogneiss. The strong change in composition and mineral inclusions from the core to the rim allowed the Authors to conclude that the metasomatic event occurred during prograde history at *P* between 1.6 GPa up to conditions close the UHP climax. Based on this study and on Cl stable isotope data on serpentinites, Sharp & Barnes (2004) proposed that the unusual bulk composition of the whiteschists, especially the high-Mg content, was due to the infiltration of high-salinity fluids generated during subduction by dehydration of antigorite from the underlying oceanic crust. In a recent paper, Schertl & Schreyer (2008), comparing whole-rock major- and trace-element data from a number of the BIU whiteschists and of the host orthogneisses/metagranites, accepted the metasomatic origin, and concluded that the whiteschists derived from a granitoid/orthogneiss protolith through a significant increase in Mg and a decrease in Na, Ca, Fe, Cu, P, Rb, Ba, and Sr. However, they did not give a conclusive explanation of the nature of the metasomatic fluid.

In this paper, we use new petrologic, geochemical, and fluid inclusion data to constrain a model for the metasomatic formation of the whiteschists and their subsequent UHP history. We devoted our study mainly to the different generations of pyrope-rich garnets and to the associated minerals and fluid inclusions present in samples collected from the classic locality of Case Ramello (i.e., Case Parigi of Chopin, 1984) and from a new sampling site located SSW of Case Ramello (Po valley).

GEOLOGICAL BACKGROUND

The Dora-Maira Massif (DMM), together with the Gran Paradiso and the Monte Rosa, belongs to the Internal Crystalline Massifs of the Pennine Domain of the Western Alps (Fig. 1a). Detailed field and laboratory investigations of the southern DMM (see Compagnoni & Rolfo, 2003, and Compagnoni *et al*., 2004 for a review) showed that this portion of the massif consists of a nappe pile composed of continent-derived tectonic units—including both the Variscan crystalline basement and its Triassic cover—juxtaposed during the Alpine orogeny to thin, ocean-derived units (calcschists and metaophiolites) of the Piemonte Zone (Fig. 1a). Among these units, only the Brossasco-Isasca Unit (BIU) experienced an early Alpine UHP metamorphism, peaking at 730 °C and 4.0–4.5 GPa (Hermann, 2003; Castelli *et al*., 2007), followed by a retrograde greenschist-facies recrystallisation. The BIU has been subdivided into a "Polymetamorphic Complex" derived from Alpine tectono-metamorphic reworking of the Variscan amphibolite-facies metamorphic basement and a "Monometamorphic Complex" consisting of orthogneiss (mainly augengneiss with very minor metagranites) derived from Alpine tectono-metamorphic reworking of Permian granitoids (Compagnoni *et al*., 1995; Fig. 1b).

The Monometamorphic Complex locally also includes peculiar Mg-rich and Na-Ca-poor lithologies, named "pyrope-whiteschists" (Fig. 1b; Compagnoni *et al*., 2004), which occur within the orthogneisses as layers from a few centimetres to about 20 metres in thickness and from a few metres to hundreds of metres in length (e.g., Compagnoni *et al*., 1995). The contact between the whiteschist and the hosting orthogneiss is marked by a few decimetres to several metres of a phengite-rich, banded gneiss locally preserving relics of the igneous K-feldspar phenocrysts (Compagnoni *et al*., 1995).

ANALYTICAL TECHNIQUES

Chemical analyses of minerals were obtained using a CAMECA SX50 electron microprobe at the IGAG, CNR of Roma. Operating conditions were 15 kV accelerating voltage, 15 nA beam current, and 10 s counting time for each element. The used natural and synthetic standards were: orthoclase (K), wollastonite (Ca, Si), native manganese (Mn), corundum (Al), jadeite (Na), magnetite (Fe), olivine (Mg), native chromium (Cr), native zirconium (Zr), rutile (Ti), apatite (P), potassium chloride (Cl), and phlogopite (F). At the above operating conditions, values below 0.05

wt% for minor elements must be considered only indicative. Areal analyses of 50–10 μm^2 have been collected on micas.

Whole-rock major- and trace-element compositions were analysed at Chemex Laboratories (Canada) using ICP-AES (major elements) and ICP-MS (trace elements). The precision for the analyses is better than 1% for major elements and better than 5% for trace elements. Trace-element patterns reported in the figures are plotted with the Petrograph software by Petrelli *et al.* (2005).

In situ trace-element analysis of minerals (garnet, white mica, ellenbergerite, Mg-dumortierite) and multiphase-solid (MS) inclusions were performed on doubly polished 100-μm-thick sections by using the Laser Ablation-Inductively Coupled Plasma-Mass Spectrometer (LA-ICP-MS) installed at the Department of Earth Sciences, University of Perugia (SMAArt facilities). The instrumentation consists of a New Wave UP213 frequency-quintupled Nd:YAG laser ablation system coupled with a Thermo Electron X7 quadrupole-based ICP-MS. All LA-ICP-MS measurements were carried out using time-resolved analysis operating in a peak jumping mode. Each analysis consisted of c. 40 s of measurement of instrumental background—i.e., analysis of the carrier gas with no laser ablation—followed by c. 60–80 s of data acquisition with the laser on. The laser-beam diameter, the repetition rate, and the laser energy density were fixed to 30–40 μm, 10Hz, and ~10 J/cm^2, respectively. Helium was preferred over argon as a carrier gas to enhance transport efficiency of ablated aerosol (Eggins *et al*., 1998). The helium carrier exiting the ablation cell was mixed with argon make-up gas before entering the ICP torch to maintain a stable and optimum excitation condition. Two main LA-ICP-MS analytical protocols have been adopted here: (1) mineral analysis on the sample surface, and (2) MS inclusions analysis in the depth of the sample. For mineral analysis, the time-resolved spectra are characterised by c. 40 s of gas background followed by c. 60 s of mineral signal. External calibration was performed using NIST SRM 610 and 612 glass standards in conjunction with internal standardization using ^{29}Si, previously determined by WDS electron microprobe following the method proposed by Longerich *et al*. (1996). Data reduction was performed using the Glitter software (van Achterbergh *et al*., 2001). The U. S. Geological Survey (USGS) reference standard BCR2G (a fused glass of the Columbia River Basalt) was analysed in each analytical run as quality control in order to assess the accuracy and the reproducibility of the analyses. Further details on the analytical method can be found in Petrelli *et al*. (2007, 2008). For MS inclusions (10–30 μm in diameter), analysis of the time-resolved spectra is characterized by c. 40 s of gas background, followed by the host-mineral (Prp II) signal for a time depending upon the depth of MS inclusions, and finally by the host-Prp II-plus-MS-inclusion signal. At the end of the MS inclusion, ablation signals return to the host-mineral values. The host-Prp II-plus-MS-inclusion signal was characterised for major and trace elements using the USGS standard BCR2G (USGS, 2009) as calibrator and normalizing the results to a fixed-oxide total following the procedure described in Guillong *et al.* (2005) and Halter *et al*. (2002). The concentration of one major element (^{29}Si) was subsequently used as the internal standard to reduce trace-element concentrations from count-per-second signals following the method proposed by Longerich *et al*. (1996). External calibration for trace elements was performed using the USGS standard reference material BCR2G (USGS, 2008) following the method proposed by Longerich *et al*. (1996). No correction for the host Prp II contribution was performed. This procedure does not allow us to obtain the real chemical composition of MS inclusions, but it does make it possible to clearly recognise elements that are enriched in MS inclusions with respect to the Prp II without performing assumptions or modelling to correct the analyses for the host-mineral contribution.

The composition of mineral phases within MS inclusions was investigated with a Cambridge Instruments SEM Stereoscan 360 equipped with an EDS Energy 200 and a Pentafet detector (Oxford Instruments) at the Department of Mineralogical and Petrological Sciences, University of Torino. Operating conditions were 15 kV accelerating voltage and 50 s counting time. SEM-EDS quantitative data (spot size = 2 μm) were acquired and processed using the Microanalysis Suite Issue 12 (INCA Suite version 4.01) then the raw data were calibrated on natural mineral standards and the ΦρZ correction (Pouchou & Pichoir, 1988) was applied.

Microthermometric measurements of fluid inclusions within doubly polished, 100-μm-thick sections were performed with a Linkam THM 600 heating-freezing stage coupled with an Olympus polarizing microscope (100-x objective) at the Department of Mineralogical and Petrological Sciences, University of Torino. The instruments were calibrated by a set of synthetic fluid inclusions (SYNFLINC) with an estimated accuracy of about ±0.1 °C at the triple point of CO_2 (-56.6 °C), at the triple point of H_2O (0.01 °C), and at the critical temperature of H_2O (374 °C). Fluid-inclusion compositions were determined by using the package FLUID (Bakker, 2003; Bakker & Brown, 2003).

Raman microspectroscopy analyses were collected at the Department of Earth Sciences of Siena (with a confocal Labram multichannel spectrometer by Jobin Yvon Instruments, characterised by an excitation line at 514.5 nm produced by an Ar^+-ion laser, a Notch holographic filter with a spectral resolution of 1.5 cm^{-1}, and a grating of 1800 grooves/mm) and at the Department of Mineralogical and Petrological Sciences of Torino (with an integrated micro/macro Raman LABRAM HRVIS by Horiba Jobin Yvon Instruments, characterised by an excitation line at 532.11 produced by solid-state Nd laser, a Super Notch Plus filter with spectral resolution of 1 cm^{-1}, and a grating of 600 grooves/mm). The beam was focused to a spot size of about 1–2 μm using a 100-x objective. The daily calibration was performed using the 1,332-cm^{-1} diamond band or the 520.6-cm^{-1} Si band.

PETROGRAPHY AND MINERAL CHEMISTRY

The studied UHP whiteschists consist of pyropes—from medium to very-coarse grain size—embedded in a matrix of variable amounts of quartz (from former coesite), kyanite, phengite, talc, and accessory rutile, apatite, zircon, and monazite. Mg-chlorite, muscovite, phlogopite, paragonite, unusual Mg-rich minerals, and accessories occur as inclusions in pyrope and/or kyanite (see below).

Three kinds of zoned **garnets** have been distinguished (Fig. 2): (1) **megablasts**—from 10 to 20 cm in diameter—characterised by a wide, reddish core (Prp I; abbreviations after Fettes & Desmons, 2007), a thin inner rim (Prp II), and a thinner outer rim (Prp III); (2) **porphyroblasts**—from 2 to 10 cm in diameter—characterised by a small Prp I core, a wide Prp II inner rim, and a thin Prp III outer rim; and (3) **neoblasts**, less than 2 cm in diameter, characterised by a wide Prp II core and a thin Prp III rim. **Prp I** ($Prp_{69-81}Alm_{16-26}$; Fig. 3a; Table 1) is interpreted as a prograde garnet (see also Schertl *et al*., 1991) because it includes kyanite, talc, phlogopite (totally retrogressed to vermiculite), a zoned ellenbergerite with little P-ellenbergerite component (Si/P = 43 in the core; Si/P = 263 in the rim), and Mg-chlorite [mg# = Mg/(Mg + Fe) = 0.95], Mg-dumortierite, rutile, zircon, apatite, and monazite, but never coesite/quartz or phengite. **Prp II** ($Prp_{82-98}Alm_{1-16}$; Fig. 3a; Table 1) is interpreted as a peak garnet (see also Schertl *et al*., 1991) because it contains inclusions of coesite, kyanite, phengite, rutile, zircon, monazite, and rare talc, but never Mg-chlorite and phlogopite. **Prp III** ($Prp_{86-67}Alm_{4-11}$; Fig. 3a; Table 1), usually pseudomorphically replaced by phengite, biotite, talc, kyanite, and chlorite (e.g., Schertl *et al*., 1991; Hermann, 2003), is considered retrograde because it includes phengite, kyanite, rutile, and zircon. All pyrope generations always contain P (up to 0.012 a.p.f.u.), Ti (locally, up to 0.008 a.p.f.u.), Zr (up to 0.004 a.p.f.u.), and Cr (up to 0.002 a.p.f.u.) and, more rarely, F (up to 0.011 a.p.f.u.) and Cl (up to 0.001 a.p.f.u.; see Table 1).

Three **kyanite** generations have been distinguished in the whiteschists: (1) prograde porphyroblastic **Ky I**, usually occurring within Prp I and including quartz, rutile, zircon, and minor talc, muscovite, paragonite, and Mg-chlorite; (2) peak porphyroblastic **Ky II**, which occurs both in the matrix and locally also in Prp II and includes phengite and polycrystalline quartz from coesite; and (3) retrograde **Ky III**, which occurs in Prp III and, together with quartz, in the rock matrix.

Three types of **white mica** have been distinguished: (1) **prograde muscovite** (Mus: Si = 3.185 a.p.f.u., Mg = 0.216, Na = 0.352, Ti = 0.014; F = 0.005, Cl = 0.001; Fig. 3b; Table 1) included in Ky I in Prp I; (2) **peak phengite** (Phg I: Si = 3.548–3.580 a.p.f.u., Mg = 0.603–0.642, Na = 0.013–0.027, F = 0.005–0.036, Cl up to 0.001; Fig. 3b; Table 1), which forms the core of coarse-grained, zoned mica-fishes in the matrix and, locally, is also included in Prp II; and (3) **retrograde phengite** (Phg II: Si = 3.495–3.540 a.p.f.u., Mg = 0.568–0.624, Na = 0.008–0.025, F =

0.009–0.037, Cl up to 0.001; Fig. 3b; Table 1), which occurs in the matrix as the rim of Phg II mica fishes and as finer-grained, retrograde neoblasts. Little P (up to 0.003 a.p.f.u.), Zr (up to 0.004 a.p.f.u.) and Cr (up to 0.002 a.p.f.u.) were locally measured in white micas (Table 1).

MAJOR- AND TRACE-ELEMENT DISTRIBUTION

Whole-rock

Whole-rock major- and trace-element compositions of two samples consisting of polycrystalline quartz, pyrope neoblasts, kyanite, phengite, and minor talc are reported in Table 2. For comparison, a sample of the hosting UHP metagranite from Brossasco is reported. The metagranite is characterised by an igneous porphyritic structure partly obliterated by Alpine coronitic and pseudomorphous metamorphic reactions. The original igneous mineral assemblage consisted of quartz, plagioclase, K-feldspar, biotite, and accessory apatite, tourmaline, zircon, and monazite. Only the igneous K-feldspar is still preserved, whereas quartz is replaced by coesite (now polycrystalline quartz); plagioclase by an aggregate of jadeite + (coesite) + zoisite + kyanite + K-feldspar; and biotite by an aggregate of Mg-richer biotite + phengite + rutile. Coronitic microstructures involving garnet are present at the contacts between biotite and quartz, between biotite and K-feldspar, and between biotite and plagioclase (for more details, see Compagnoni *et al*., 1995).

With respect to the Brossasco metagranite, which is a normative peraluminous granite (CIPW norm), the UHP whiteschists are remarkably enriched in MgO and show an important depletion in Na_2O, K_2O and CaO; SiO_2 and Al_2O_3 contents are similar in the two lithologies.

Figure 4 shows the trace-element patterns of the two UHP whiteschists and the metagranite normalised with respect to the primordial mantle (PM; McDonough & Sun, 1995). For comparison, the composition of the average continental crust from Rudnick & Gao (2005) is also reported. With respect to the average continental crust, the metagranite shows selective, strong enrichments in Cs, Rb, and Pb, moderate enrichments in Th, U, and K, and depletions in Ba, Sr, Eu, and Ti. The two whiteschists show depletion in Sr with respect to the PM. With respect to the average continental crust, they show moderate enrichments in Th, U, HREE (Dy, Yb, and Lu), Y—and one sample also in Hf and Zr—and depletions in Ba, Sr, Eu, and Ti. With respect to the metagranite, the patterns are enriched in HREE, Y, and, in one sample, in Hf and Zr, and they are depleted in LILE (Cs, Pb, Rb, K, Sr, Ba).

Minerals

Trace-element compositions of garnet (Prp II), white mica (Mus, Phg I, and Phg II), Mg-dumortierite (Dum), and ellenbergerite (Ell) have been determined (Table 3 and Fig. 5), whereas quartz, kyanite, and talc have not been considered because they are not significant carriers of trace elements.

With respect to the PM, Prp II is enriched in HREE (Dy, Yb, Lu), Y, and Eu, with some variations observed among samples (Fig. 5a). Rb and Sm values are near the PM, whereas the other elements are lower than the PM. White micas are strongly enriched in Rb, Cs, and Pb, and moderately enriched in Ba, Ta, U, and Nb (Fig. 5b). In particular, retrograde Phg II is enriched in Th, whereas prograde Mus and Phg I are Th-depleted. Mg-dumortierite is strongly enriched in Hf, Zr, and U, whereas it is strongly depleted in Th, Yb, La, and Y (Fig. 5c). The ellenbergerite core is strongly enriched in U, Zr, and Hf, moderately enriched in Nb, Th, and Ta, scarcely enriched in Ti, HREE, Y, and Pb, and depleted in Sm, Eu, K, Nd, LREE (La, Ce), Ba, and Sr (Fig. 5c). The ellenbergerite rim is characterised by an increase in Ta and Nb and a decrease in the other elements, in particular Hf, Zr, U, Th, HREE, and Y, with respect to the ellenbergerite core (Fig. 5c).

FLUID-INCLUSION STUDY

Type I: Fluid inclusions in Ky I

Primary fluid inclusions have been found only within three grains of prograde Ky I. Primary inclusions, about 40 μm in length, show negative crystal shape, and their distribution is parallel to the kyanite elongation. They are three-phase (S + L + V) aqueous inclusions (Fig. 6a). About 40% of the total volume consists of L + V [df = L/(L + V) = 70)], the remaining 60% being represented

by solid phases. Colourless minerals showing lamellar habit, identified as paragonite by microRaman investigations, are always present. Rarely, a colourless mineral with hexagonal habit, identified by microRaman investigations as probably being ellenbergerite, is also present.

During microthermometric measurements, the liquid phase froze between -46 and -40 °C. The first melting was observed between -31 and -28 °C—i.e., close to the eutectic of the $MgCl_2$-NaCl-H_2O system and the final melting of ice between -5.7 and -3.4 °C. During heating, a salt dissolved at 115 °C in one inclusion. The homogenization into the liquid was obtained between 232.9 and 286.8 °C. Calculated salinities range from 6 to 28 $NaCl_{eq}$ in wt%.

Type II: Multiphase-solid inclusions within Prp II

Primary multiphase-solid (MS) inclusions—i.e., a peculiar kind of "fluid" inclusion containing many different solid phases ± a fluid phase, recently found in peak minerals from several UHP terranes worldwide (cf., Ferrando *et al*., 2005)—occur within peak Prp II of both porphyroblasts and neoblasts and can represent up to 5–10 % of the total volume of the host crystal. The MS inclusions are regularly distributed and, locally, mark growth zones (Fig. 6b). They have homogeneous dimensions (from 10 to 30 μm in diameter, rarely up to 60 μm) and negative crystal shapes. Local evidence for post-entrapment decrepitation is suggested by the presence of haloes of tiny inclusions around MS inclusions with star-like habit (Fig. 6c).

Under the microscope, all MS inclusions consist of aggregates of solids (Fig. 6d), which have been identified by SEM-EDS and Raman microspectroscopy. MS inclusions lacking evidence of re-equilibration mainly contain interlayered Mg-chlorite (colourless lamellar crystals with moderate refractive indices and very low birefringence) and Na-K-phlogopite (colourless lamellar crystals with moderate refractive indices and high birefringence; Figs. 6d and 6e). Other solids, always present as minor components, are a Cl-rich apatite (equant colourless crystals with moderate refractive indices and low birefringence) and a Zn-rich pyrite (equant opaque mineral) (Fig. 6d). On freshly-broken surfaces, very small chloride crystals have been locally recognised by SEM-EDS. All of these minerals show similar dimensions and equilibrium microstructures. For this reason, they have been interpreted as daughter minerals—i.e., minerals precipitated from the fluid after entrapment. Talc and magnesite with variable sizes are found on the cavity walls of some MS inclusions, and they have been interpreted as step-daughter minerals—i.e., minerals formed by post-trapping reactions between the host mineral and fluid. More rarely, rutile, zircon, and monazite were also occasionally recognised. Their large dimensions (Fig. 6f), irregular habit, and structural relationships with the daughter minerals deny a precipitation from the fluid, but suggest mechanical entrapment together with the fluid, during the growth of Prp II.

The abundance of hydrous daughter and step-daughter minerals suggest a water-dominated fluid system, and Fourier transform infrared synchrotron radiation (FTIR) maps indicate that molecular water is preserved within single inclusions (Frezzotti *et al*., 2007b). A semi-quantitative composition of the solutes contained in the fluid within the MS inclusions was obtained by averaging Vol% of daughter minerals and empty spaces in 24 inclusions, following the method described in Ferrando *et al*. (2005). The calculated average fluid composition corresponds to SiO_2 (29 wt%), MgO (25.5 wt%), and Al_2O_3 (23 wt%), along with minor amounts of Fe_2O_3 (4.7 wt%), S (3.2 wt%), Na_2O (1.3 wt%), CaO (0.6 wt%), P_2O_5 (0.4 wt%), K_2O (0.2 wt%), Cl (0.1 wt%), Zn (< 0.1 wt%), and CO_2 (< 0.1 wt%); water bonded in hydrous minerals totals to 12.5 wt%. Probably, part of the original water contained in the MS inclusions was lost during decompression, as suggested by the presence of tiny fluid inclusions around decrepitated MS inclusions (Fig. 6c). Local, post-trapping chemical re-equilibrations between MS inclusions and the host garnet are confirmed by the increase in almandine component ($Prp_{61-69}Alm_{24-30}$) of Prp II around some MS inclusions.

Table 4 and Fig. 7 show the results of in situ LA-ICP-MS analyses performed on MS inclusions and on Prp II (see Fig. 5a). Trace-element patterns of MS inclusions plus Prp II are relatively homogeneous and characterised by strong enrichments in LILE (Pb, Cs, Sr, Rb, K) and U, depletions in HFSE (Ti, Zr, Hf, Ta, Nb), and depletions or scarce enrichments in LREE (La, Ce,

Pr), Ba, Th, and Sm with respect to the primordial mantle. From the patterns of Fig. 7, a clear enrichment in LILE (Pb, Cs, Sr, Rb, K, LREE, Ba), U and Th in the MS inclusions plus Prp II patterns with respect the host Prp II is evident.

DISCUSSION

Metamorphic evolution and *P-T* path

The present petrological and minerochemical data on BIU whiteschists are in agreement with previous works (e.g., Schertl *et al*., 1991; Compagnoni *et al*., 1995; Philippot *et al*., 1995; Hermann, 2003), and allow us to further constrain their metamorphic evolution (Fig. 8) and *P-T* path from prograde to early decompression stages (Fig. 9).

Mineral compositions from this study and previous works (Chopin, 1984; Schreyer, 1985; Chopin, 1986; Chopin *et al*., 1986; 1991; Schertl *et al*., 1991; Compagnoni *et al*., 1995; Chopin & Schertl, 1999; Compagnoni & Hirajima, 2001; Hermann, 2003) show some variations among samples, that may be due to small differences in the protolith chemistry and/or in the metasomatic process. Combining all available petrological data, five metamorphic stages (named A to E) can be distinguished (Fig. 8).

The earliest prograde stage (stage A), first described by Compagnoni & Hirajima (2001), is recorded by the growth of the almandine core of superzoned garnets discovered in whiteschists and interpreted as evidence of the occurrence of former basement xenoliths within the metagranite (see above). A P of about 1.6 GPa and a $T < 600$ °C have been inferred for this stage by these Authors. The subsequent stage B is recorded by the relict mineral assemblage preserved within Prp I, consisting of Mg-chlorite, talc, muscovite, and rare paragonite, rutile, and zircon. Ky I probably started to grow during this stage, and quartz was the stable silica polymorph in the matrix. Pressure conditions of stage B, so far poorly constrained (e.g., Schertl *et al*., 1991), have been inferred from the variation of the celadonite content in white mica, as experimentally determined in the KMASH system by Hermann (2003). The compositions of white micas preserved in Ky I within Prp I, determined in the present study (Si = 3.19 a.p.f.u.) and reported by Schertl *et al*. (1991; Si = 3.26), indicate pressures in the range 1.7–2.1 GPa. Temperatures for stage B can be inferred from the most recent *P-T* path proposed for the Case Ramello UHP whiteschists by experimental petrology (Hermann, 2003). This *P-T* path, well constrained from the metamorphic peak to the late exhumation stages, is consistent with the recent BIU *P-T* paths obtained from both marbles (Ferraris *et al*., 2005; Castelli *et al*., 2007) and eclogites (Groppo *et al*., 2007). Therefore, for prograde stage B, temperatures of about 560 and 590 °C, respectively, can be obtained for the two values of the calculated pressures (Fig. 9).

During stage C, the mineral assemblage consisted of Prp I, Ky I, talc, phlogopite, the Mg-rich minerals ellenbergerite, Mg-dumortierite, and bearthite, local jadeite and glaucophane (Fig. 8), and accessory rutile, zircon, monazite, apatite, tourmaline, and As-pyrite. During this stage, the breakdown of Mg-chlorite to give ellenbergerite and Prp I (according the reactions Chl + Ky + Tlc + Rut = Ell and Ky + Chl + Tlc = Grt + fluid; e.g., Schertl *et al*., 1991) and of muscovite to give phlogopite (according to the reaction Chl + Mus = Ky + Phl + Tlc + fluid; Hermann, 2003), occurred. *P-T* conditions of stage C are poorly constrained. The reaction curves Chl + Mus = Ky + Phl + Tlc + fluid and Ky + Chl + Tlc = Grt + fluid calculated by Hermann (2003) suggest $2.3 \leq P \leq 2.8$ GPa and $600 \leq T \leq 650$ °C (Fig. 9), whereas previous studies by Schertl *et al*. (1991) and Simon *et al*. (1997) gave $T = 700$–720 °C and $P = 2.9$–3.0 GPa. However, all of these values should be considered as maximum values because the reaction curves used to constrain the *P-T* conditions were obtained for $a_{H2O} = 1$, whereas $a_{H2O} = 0.4$–0.75 during the pyrope growth was estimated by Sharp *et al*. (1993) and a_{H2O} not exceeding 0.8–0.7 is proposed in this study on the basis of the high-salinity fluid preserved in Ky I (see below). Because with decreasing a_{H2O} the stability fields of garnet and of phlogopite extend toward lower pressures and temperatures, *P-T* conditions for stage C could be better constrained at $2.1 < P < 2.8$ GPa and $590 < T < 650$ °C—i.e., at the quartz-to-coesite transition.

At the peak stage D, the mineral assemblage consisted of Prp II, Ky II, Phg I, coesite, and accessory rutile, zircon, monazite, and tourmaline (Fig. 8). The prograde phlogopite and talc of stage C were consumed by reactions producing Prp II and Phg I, such as Phl + Ky + Tlc = Grt + Phg + fluid, and Ky + Tlc = Grt + Coe + fluid (Schertl *et al*., 1991; Hermann, 2003). While the peak temperature remained constrained at about 730 °C, through the years the calculated peak pressure progressively increased from 3.7 GPa (Schertl *et al*., 1991) to 4.3 ± 0.3 GPa (Hermann, 2003), which is in agreement with the peak pressure of 4.0 GPa recently estimated from marbles (Castelli *et al*., 2007).

The early decompression stage E, with a mineral assemblage consisting of coesite, Prp III, Ky III, Phg II, and talc, was constrained at about 720 °C by Hermann (2003) and at 3.6–3.9 GPa on the basis of composition of Phg II.

Fluid-phase evolution

Two distinct generations of fluids (type I and type II) have been characterised by the fluid-inclusion study. Type-I fluid is preserved in primary fluid inclusions within Ky I. The fluid distribution in Ky I and the presence of ellenbergerite, as an incidentally trapped mineral, indicate that type I is a prograde fluid trapped during metamorphic stage C. It is an NaCl-$MgCl_2$-rich brine, with salinity varying from 6 to 28 $NaCl_{eq}$ (in wt%), and the presence of paragonite as a daughter mineral indicates that the fluid also contained Si and Al as dissolved cations. The presence of daughter paragonite does not allow us to calculate readily the corresponding water activities, which should have been below 0.8. Hermann (2003) and Hermann *et al*. (2006) suggested that in the BIU the fluid phase at *P-T* conditions compatible with stage C should have contained 10–20 wt% of total dissolved solids (Fig. 9). The present fluid-inclusion study suggests that, in the whiteschists, the weight percentage of dissolved solids in type-I fluid was higher because of the solubility increase of cations such as Si and Al.

The primary MS inclusions within Prp II are remnants of the fluid phase (type II) present in the system during the UHP metamorphic peak. The semi-quantitative composition of the fluid obtained by the study of MS inclusions is probably affected by an over-estimation of MgO because of the chemical re-equilibrations that occurred between the MS inclusions and the host garnet after the entrapment. However, the MS inclusions are representative of an aqueous solution with low a_{H2O} because of the high contents of solutes.

This is an alumino-silicate aqueous solution with composition intermediate between an aqueous fluid and a silicate melt. The experimental work of Hermann (2003) demonstrated that peak metamorphic conditions reached by the BIU whiteschists have been higher than the second critical end-point for a granitic system and suggested that, at these *P-T* conditions, the liquid phase should have contained up to 50 % of dissolved species (values of about 60–65 % can be deduced from Fig. 9).

The fluid-inclusion study reveals important differences between the prograde type-I fluid and the peak type-II fluid. Both fluids are aqueous and contain Na, Mg, Cl, Al, and Si as main dissolved cations, but their chemical and physical properties are different. In fact, despite the presence of dissolved Al and Si, prograde type-I fluid is an $MgCl_2$-rich brine. In contrast, type-II fluid mostly consists of Si and Al, whereas the Cl content is subordinate. In addition, type-II fluid also contains relatively high amounts of Ca, which is not present in type-I fluid.

In a previous fluid-inclusion study of BIU whiteschists, Philippot *et al.* (1995) described the presence in pyrope megablasts of complex inclusions consisting of magnesite, Mg-phosphate, chloride, talc or Mg-chlorite, and an opaque mineral—representative of a brine composed of H_2O, CO_2, Cl, P, Mg, Na or K, Si and Al. The composition of this fluid is different with respect to our type-II fluid that is characterised by lower H_2O and Cl contents, higher Si and Al contents, and by the presence of Ca. These differences could indicate either 1) a different post-trapping re-equilibration of the same fluid, or 2) a high variability in the fluid chemistry from prograde (HP) to peak (UHP) conditions.

Though Philippot *et al.* (1995) did not distinguish the different generations of garnet, on the basis of the petrographic description we can suppose that the fluid inclusions are hosted in the large core of the megablasts, i.e. in Prp I (see Fig. 2). In our samples, fluid inclusions similar to those described by Philippot *et al.* (1995) are absent, not only in prograde Prp I garnets but also in the other rock-forming minerals. Similarly, Philippot *et al.* (1995) did not report in their samples the presence of fluid inclusions with composition and distribution similar to our type II MS inclusions. This implies that the differences in composition between the two fluids cannot be due to a different fluid inclusion re-equilibration.

The complex inclusions described by Philippot *et al.* (1995) have composition intermediate between our type-I and type-II fluids, so that present and previous fluid inclusion studies allow us to delineate a progressive and continuous transition from prograde Cl-dominated aqueous fluids to peak alumino-silicate aqueous solution at increasing pressure.

Element mobility

The comparison of whole-rock major- and trace-element abundance between whiteschists and host metagranite leads us to evaluate the element mobility. Whereas Si and Al remained unchanged, enrichment in Mg and depletion in alkalies, Ca, Fe, and possibly P in the whiteschists with respect to the granitoid protolith indicates that they originated from the hosting metagranite by a metasomatic process, as has recently been suggested by the geochemical study of Schertl & Schreyer (2008). As for trace elements, the depletion in LILE (Cs, Pb, Rb, Sr, Ba; cf. Fig. 4) shown by whiteschists with respect to the hosting metagranite is consistent with the observed decrease in alkalies and Ca. The enrichments in HREE (Dy, Yb, Lu), Y, and, locally, Hf and Zr, with respect to the hosting metagranite are related to the growth in the whiteschists of garnet, ellenbergerite, and Mg-dumortierite, minerals which strongly partitioned these elements (see Fig. 5). These data indicate that the whiteschist history consisted not only of metamorphic but also, and especially, of metasomatic events caused by the influx of a fluid carrying Mg, leaching alkalies, Ca and LILE.

UHP whiteschists from the BIU: An example of crustal metasomatism during subduction

Pre-Alpine and prograde Alpine evolution

It is well established that at about 275 Ma ago (Gebauer *et al.,* 1997) large volumes of granitoids intruded into the Variscan metamorphic basement now exposed in the Internal Crystalline Massifs of Monte Rosa, Gran Paradiso, and Dora-Maira. At the intrusive contacts, the country rocks were locally fragmented, and some fragments were caught up in the magma as xenoliths (e.g., Compagnoni & Rolfo, 2003). During the Alpine subduction, both granitoids and basement xenoliths underwent prograde HP metamorphism, and in the xenoliths of suitable composition an almandine-rich garnet started to grow (Stage A in Fig. 10). Compagnoni & Hirajima (2001) report the presence, within xenoliths, of superzoned garnets consisting of an almandine-rich core, compatible with the bulk chemistry of a xenolith, and a pyrope-rich rim, compatible with the bulk chemistry of the including whiteschist. The prograde HP stage A, recorded not only by the zoning of the almandine-rich core but also by its inclusions of staurolite, chloritoid, and chlorite (mg# = 0.60–0.80), is constrained at $P \sim 1.6$ GPa and $T \leq 600$ °C (Compagnoni & Hirajima, 2001). The mineral assemblage stable during stage A indicates that the metasomatic process responsible for the formation of whiteschists could not have taken place yet.

The relevant Mg-increase and Ca and Na depletion in both metagranite and xenoliths, undoubtedly occurred during stage B (1.7–2.1 GPa and 550–590 °C; Fig. 10), as testified, respectively, by the prograde inclusions of talc and Mg-chlorite (mg# = 0.85–0.99: Schertl *et al.*, 1991; Compagnoni & Hirajima, 2001) in the Prp I of our whiteschists and by the prograde inclusions of Mg-chlorite (mg# = 0.85: Compagnoni & Hirajima, 2001) in the pyrope-rich rim of superzoned garnet. The sharp change in the bulk rock chemistry of the former xenolith toward whiteschist composition during stage B caused partial reabsorption of the almandine garnet (see the irregular and corroded shape of the almandine-rich core in Fig. 5 of Compagnoni & Hirajima, 2001) and promoted the growth of Mg-chlorite.

Prograde stage C ($2.1 < P < 2.8$ GPa and $590 < T < 650$ °C; Fig. 10) was characterised by the progressive and continuous growth of the Mg-rich phases—e.g., Prp I and ellenbergerite—at the expense of Mg-chlorite. During stage C, pyrope rim overgrew the corroded almandine-rich core of the superzoned garnets in whiteschists from former xenoliths. In whiteschists with granitic protholith, the development of the unusually large Prp I cores in the megablasts was likely a consequence of a high fluid/rock ratio and suggests that the metasomatic process should have been still active during stage C, at pressures close to transition between HP and UHP conditions. Type-I fluid inclusions trapped during stage C indicate that the fluid phase was a $MgCl_2$-rich brine.

The Compagnoni & Hirajima (2001) interpretation, that the presence of superzoned garnets marks the significant change in the rock bulk chemical composition connected to a metasomatic event occurred under prograde Alpine metamorphism (from pressures above 1.6 GPa to conditions close the UHP climax) along shear zones, was further supported by the Cl stable-isotope data of Sharp & Barnes (2004). These Authors proposed that the BIU whiteschists formed by the channelised infiltration into granitoid/orthogneiss of brines generated during serpentinite dehydration of subducting oceanic lithosphere, tectonically underlying the Dora-Maira Massif. Based on the Cl-content of serpentines, they suggested the presence of a Mg- and Cl- rich fluid released from the antigorite breakdown, in agreement with a number of independent lines of evidence from fluid inclusion studies (e.g. Scambelluri *et al*., 2001). Sharp & Barnes (2004) further demonstrated that the high amount of chlorine present in the subducting serpentinites reduces the a_{H2O} in the system and that the release of brines should have occurred over a relatively wide range of *P-T* conditions, because the temperature of the main serpentinite dehydration reaction Atg = Ol + Opx + fluid depends upon the a_{H2O}.

The present finding of prograde Mg- and Cl-rich brines during stage C not only supports a similar model, but also further constrains the *P-T* conditions of the metasomatic evolution (stages B and C). In Fig. 9, the curves of the antigorite breakdown for three water activities (0.50, 0.75, and 1.00) reported by Sharp & Barnes (2004) are superimposed on the *P-T* path of the UHP whiteschists. From this figure, it is evident that during stages B and C the BIU may have been infiltrated by Mg- and Cl- rich fluids progressively generated by the antigorite breakdown. The depletion in incompatible trace elements observed in the whiteschists also fits this model because of the negligible capacity of serpentine, such as other hydrous Mg-silicates, to store and, then, to release significant amount of LILE during dehydration (Zack & John, 2007).

UHP metamorphic climax

At the UHP metamorphic peak (stage D in Fig. 10; constrained at 4.0–4.3 GPa and 730 °C, and dated at 35 Ma by Tilton *et al.*, 1989; Duchêne *et al.*, 1997; Gebauer *et al.*, 1997; Vaggelli *et al.*, 2006), Prp II overgrew as rim of megablasts and as core of small neoblasts. The climax metamorphic fluid was an alumino-silicate aqueous solution, with composition intermediate between an aqueous fluid and a silicate melt, enriched in Si, Al, Mg, Fe, S, alkalies, Ca and LILE, but with only traces of Cl. Fluid/rock chemical equilibrium was achieved at the UHP conditions, as is shown by the trace-element partitioning among MS inclusions (Fig, 7), Prp II (HREE and Y in Fig. 5a), and peak phengite (e.g., Ba and Rb/Cs ratio in Fig. 5b; Melzer & Wunder, 2000).

Trace-element composition of the UHP fluid is consistent with the crustal signature retained by the UHP whiteschists (compare Figs. 7 and 4). Petrogenetic grids in the KMASH system (Hermann, 2003) indicate that peak Prp II formed by dehydration reactions, such as Phl + Ky + Tlc = Grt + Phg + fluid, and Ky + Tlc = Grt + Coe + fluid. If this was the case, the high amounts of Si, Al, and Mg in the type-II fluid could have been due to the talc + kyanite breakdown reaction, whereas the presence of K, Na, and LILE could have been due to the phlogopite breakdown reaction. Fe, S, Ca, and P probably derived by destabilisation of accessory pyrite and apatite.

Previous petrological and stable-isotope studies on UHP whiteschists also concluded in favour of an internal origin for the peak fluid (e.g., Sharp *et al*., 1993; Chopin & Schertl, 1999). The internal origin would indicate the end of the influx of brines released from antigorite dehydration, in agreement with petrological modelling, as is evident from Fig. 9, where the antigorite breakdown

curves intersect the *P-T* path well below the peak conditions. Thus, if external influx of fluid had continued also at this stage, its role would have been chemically negligible.

CONCLUSIONS

The UHP whiteschists from BIU preserve evidence for a pervasive metasomatic event during prograde HP metamorphism connected to subduction. The studied whiteschists are mainly characterised by an increase in Mg and a decrease in alkalies, Ca and Fe with respect to the metagranite protolith. Petrological, geochemical, and fluid-inclusion data point to a metasomatic fluid consisting of Mg-rich brines generated from the antigorite breakdown in subducting oceanic lithosphere and infiltrating the overlying granitoids along shear zones. In contrast, the MS inclusions within UHP pyrope (Prp II) are indicative of an internally derived, LILE-enriched, alumino-silicate aqueous solution intermediate between an aqueous fluid and a silicate melt, released from the whiteschists during prograde evolution close to the metamorphic peak.

The same metasomatic process that generated the Dora-Maira whiteschists could have also generated other lithologies, characterised by very-high Mg content and low Ca, Na, and/or K contents, which occur within granitoids and are known as “silvery micaschists” in the Dora-Maira (e.g., Cadoppi, 1990), Gran Paradiso (e.g., Dal Piaz & Lombardo, 1986) and Monte Rosa Massifs (e.g., Pawling & Baumgartner, 2001), or as “leucophyllites” from the Central-Eastern Alps (e.g., Demény *et al*., 1997; Barnes *et al*., 2004). Other lithologies may also have been affected by Mg-metasomatism, but heterogeneities in protolith composition and structure may hinder recognition of the metasomatic signal in rocks other than massive orthogneisses.

Finally, our study shows that at pressures higher than about 2.5 GPa the aqueous fluid phase changes its chemical properties, in absence of melting processes. At increasing pressure, the aqueous fluid becomes able to dissolve high amounts of cations (particularly Si and Al) involved in metamorphic reactions, while the Cl content progressively decreases, with respect to the brines stable at lower pressures. Above 3.5 - 4 GPa the aqueous fluid phase in equilibrium with the metamorphic rocks is alumino – silicate rich, and contains only negligible chlorine. The increasing evidence for generation of these alumino-silicate aqueous solutions in continental lithologies during deep subduction (e.g., Hermann *et al*., 2006; Frezzotti *et al*., 2007a) suggests that the fluids, showing LILE enrichment and HFSE depletion, could represent important metasomatic agents for the release of incompatible trace elements into the supra-subduction mantle wedge.

ACKNOWLEDGEMENTS

We are grateful to M. Beltrando, I. Gabudianu, and C. Groppo for constructive discussions. We thank T. Hirajima and J. Selverstone for their thoughtful and detailed reviews and comments, and L. Dobrzhinetskaya for editorial handling of the manuscript. This work was financially supported by a grant from the University of Torino to R.C., and from the University of Siena to M.L.F. (PAR 2006). Raman facility in Siena was provided by the Italian Program for Research in Antarctica (P.N.R.A.). Raman facility in Torino was provided by the Interdepartmental Center “G. Scansetti” for Studies on Asbestos and Other Toxic Particulates, funded by the Compagnia di San Paolo, Torino.

REFERENCES

Bakker, R. J., 2003. Package FLUIDS 1. Computer programs for analysis of fluid inclusion data and for modelling bulk fluid properties. *Chemical Geology*, **194**, 3–23.

Bakker, R. J. & Brown, P., 2003. Computer modelling in fluid inclusion research. In: *Fluid inclusions: analysis and interpretation* (eds Samson, I., Anderson, A. & Marshall, D.), *Mineralogical Association of Canada*, Short Course Series, **32**, 175–212.

Barnes, J. D., Selverstone, J. & Sharp, Z.D., 2004. Interactions between serpentinite devolatilization, metasomatism and strike-slip strain localization during deep-crustal shearing in the Eastern Alps. *Journal of Metamorphic Geology*, **22**, 283–300.

Cadoppi, P., 1990. Geology of the crystalline basement from the northern sector of the Dora-Maira Massif, western Alps. *PhD Thesis, University of Torino (Italy)*, 208 pp. (in Italian).

Castelli, D., Rolfo, F., Groppo, C. & Compagnoni, R., 2007. Impure marbles from the UHP Brossasco-Isasca Unit (Dora-Maira Massif, western Alps): evidence for Alpine equilibration in the diamond stability field and evaluation of the X(CO_2) fluid evolution. *Journal of Metamorphic Geology*, **25**, 587–603.

Chopin, C., 1984. Coesite and pure pyrope in high-grade blueschists of the western Alps: a first record and some consequences. *Contributions to Mineralogy and Petrology*, **86**, 107–118.

Chopin, C., 1986. Phase relationships of ellenbergerite, a new high-pressure Mg-Al-Ti-silicate in pyrope-coesite-quartzite from the Western Alps. In: Blueschists and related eclogites (eds Evans, B.W. & Brown, E.H.), *Geological Society of America Memoir*, **164**, 31–42.

Chopin, C. & Ferraris, G., 2003. Mineral chemistry and mineral reactions in UHPM rocks. In: *Ultrahigh Pressure Metamorphism* (eds Carswell, D.A. & Compagnoni, R.), *EMU Notes in Mineralogy*, **5**, 191–227.

Chopin, C., Ferraris, G., Ivaldi, G., Schertl, H.-P., Schreyer, W., Compagnoni, R., Davidson, C. & Davis, A.M., 1995. Magnesiodumortierite, a new mineral from very-high-pressure rocks (western Alps). Part II. Crystal chemistry and petrological significance. *European Journal of Mineralogy*, **7**, 525–535.

Chopin, C., Henry, C. & Michard, A., 1991. Geology and petrology of the coesite–bearing terrane, Dora Maira massif, Western Alps. *European Journal of Mineralogy*, **3**, 263–291.

Chopin, C., Klaska, R., Medenbach, O. & Dron, D., 1986. Ellenbergerite, a new high pressure Mg-Al-(Ti, Zr)-silicate with a novel structure based on face-sharing octahedra. *Contributions to Mineralogy and Petrology*, **92**, 316–321.

Chopin, C. & Schertl, H.-P., 1999. The UHP Unit in the Dora-Maira massif, western Alps. *International Geology Review*, **41**, 765–780.

Compagnoni, R. & Hirajima, T., 1992. Occurrence and significance of superzoned garnet in the coesite-bearing whiteschists of southern Dora-Maira, Western Alps. 29th IGC, Kyoto, *Abstr.*, **2**, 599.

Compagnoni, R. & Hirajima, T., 2001. Superzoned garnets in the coesite-bearing Brossasco-Isasca Unit, Dora-Maira massif, Western Alps, and the origin of the whiteschists. *Lithos*, **57**, 219–236.

Compagnoni, R., Hirajima, T, & Chopin C., 1995. Ultra-High-Pressure Metamorphic Rocks in the Western Alps. In: *Ultrahigh Pressure Metamorphism* (eds Coleman, R. G. & Wang, X.), pp. 206–243. Cambridge University Press, Cambridge.

Compagnoni, R. & Rolfo, F., 2003. UHPM units in the Western Alps. In: *Ultrahigh Pressure Metamorphism* (eds Carswell, D.A. & Compagnoni, R.), *EMU Notes in Mineralogy*, **5**, 13–49.

Compagnoni, R., Rolfo, F., Groppo, C., Hirajima, T. & Turello, R., 2004. Mapping of Alpine rocks characterized by “HP” to “UHP” metamorphic overprint in the Southern Dora-Maira Massif (Western Alps). In: *Mapping Geology in Italy* (eds Pasquarè , G., Venturini, C. & Groppelli, G.), *APAT-Dipartimento Difesa del Suolo, Servizio Geologico d’Italia, Roma, Map 34*, pp. 287–294. Printed by S.EL.CA., Firenze.

Dal Piaz, G. V. & Lombardo, B., 1986. Early Alpine eclogite metamorphism in the Penninic Monte Rosa - Gran Paradiso basement nappes of the north-western Alps. *Geological Society of America Memoir*, **164**, 249–265.

Demény, A., Sharp, Z. D. & Pfeifer, H. R., 1997. Mg-metasomatism and formation conditions of Mg-chlorite-muscovite-quartzphyllites (leucophyllites) of the Eastern Alps (W. Hungary) and their relations to Alpine whiteschists. *Contributions to Mineralogy and Petrology*, **128**, 247–260.

Duchêne, S., Blichert-Toft, J., Luais, B., Télouk, P., Lardeaux, J. M. & Albarède, F., 1997. The Lu-Hf dating of garnets and the ages of the Alpine high-pressure metamorphism. *Nature*, **387**, 586–589.

Eggins, S. M., Kinsley, L. P. J. & Shelley, J. M. G., 1998. Deposition and fractionation processes during atmospheric pressure laser sampling for analysis by ICP-MS. *Applied Surface Science*, **129**, 278–286.

Ferrando, S., Frezzotti, M. L., Dallai, L. & Compagnoni, R., 2005. Multiphase solid inclusions in UHP rocks (Su-Lu, China): remnants of supercritical silicate-rich aqueous fluids released during continental subduction. *Chemical Geology*, **223**, 68–81.

Ferraris, C., Castelli, D. & Lombardo, B., 2005. SEM/TEM-AEM characterization of micro- and nano-scale zonation in phengite from a UHP Dora-Maira marble: petrologic significance of armoured Si-rich domains. *European Journal of Mineralogy*, **17**, 453–464.

Fettes, D. & Desmons, J. (eds), 2007. Metamorphic rocks. A classification and glossary of terms. Recommendations of the International Union of Geological Sciences Subcommission on the systematics of metamorphic rocks. Cambridge University Press, Cambridge, U.K., 244 pp.

Frezzotti, M. L., Ferrando, S., Dallai, L. & Compagnoni, R., 2007a. Intermediate alkali–alumino–silicate aqueous solutions released by deeply subducted continental crust: fluid evolution in UHP OH–rich topaz–kyanite quartzites from Donghai (Sulu, China). *Journal of Petrology*, **48**, 1219–1241.

Frezzotti, M. L., Tecce, F., Perucchi, A., Ferrando, S. & Compagnoni, R., 2007b. Infrared imaging of H_2O concentrations in nominally anhydrous minerals containing fluid inclusions, using synchrotron radiation. European Current Research On Fluid Inclusions (ECROFI XIX), Bern, Switzerland*, Abstract Volume*, 122.

Gebauer, D., Schertl, H.-P., Brix, M. & Schreyer, W., 1997. 35 Ma old ultrahigh-pressure metamorphism and evidence for very rapid exhumation in the Dora Maira Massif, Western Alps. *Lithos*, **41,** 5–24.

Groppo, C., Lombardo, B., Castelli, D. & Compagnoni, R., 2007. Exhumation history of the UHPM Brossasco-Isasca Unit, Dora-Maira Massif, as inferred from a phengite-amphibole eclogite. *International Geology Review*, **49**, 142–168.

Guillong, M., Hametner, K., Reusser, E., Wilson, S. A., Günther, D., 2005. Preliminary characterisation of new glass reference materials (GSA-1G, GSC-1G, GSD-1G and GSE-1G) by Laser Ablation-Inductively Coupled Plasma-Mass Spectrometry using 193 nm, 213 nm and 266 nm wavelengths. *Geostandards and Geoanalytical Research*, **29**, 315–331.

Halter, W. E., Pettke, T., Heinrich, C. A. & Rothen–Rutishauser, B., 2002. Major to trace element analysis of melt inclusions by laser-ablation ICP-MS: methods of quantification. *Chemical Geology*, **183**, 63–86.

Hermann, J., 2003. Experimental evidence for diamond-facies metamorphism in the Dora Maira massif. *Lithos*, **70**, 163-182.

Hermann, J., Spandler, C., Hack, A. & Korsakov, A. V., 2006. Aqueous fluids and hydrous melts in high-pressure and ultra-high pressure rocks: implications for element transfer in subduction zones. *Lithos*, **92**, 399–417.

Longerich, H. P., Jackson, S. E., & Günther, D., 1996. Inter-laboratory note. Laser ablation-inductively coupled plasma mass spectrometric transient signal data acquisition and analyte concentration calculation. *Journal of Analytical Atomic Spectrometry*, **11**, 899–904.

McDonough, W. F. & Sun, S.-S., 1995. The composition of the Earth. *Chemical Geology*, **120**, 223–253.

Melzer, S. & Wunder, B., 2000. Island-arc basalt alkali ratios: constraints from phengite-fluid partitioning experiments. *Geology*, **28**, 583-586.

Newton, R. C. & Manning, C. E., 2000a. Quartz solubility in H_2O-NaCl and H_2O-CO_2 solutions at deep crust-upper mantle pressures and temperatures: 2–15 kbar and 500–900°C. *Geochimica et Cosmochimica Acta*, **64**, 2993–3005.

Newton, R. C. & Manning, C. E., 2000b. Metasomatic phase relations in the system CaO–MgO–SiO_2–H_2O–NaCl at high temperatures and pressures. *International Geology Review,* **42**, 152–162.

Pawling, S. & Baumgartner, L. P., 2001. Geochemistry of a talc-kyanite-chloritoid shear zone within the Monte Rosa granite, Val d'Ayas, Italy. *Schweizerische Mineralogische und Petrographische Mitteilungen*, **81**, 329–346.

Petrelli, M., Perugini, D., Poli, G. & Peccerillo, A., 2007. Graphite electrode tetraborate fusion for automated trace element determination in bulk samples by laser ablation ICP-MS. *Microchimica Acta*, **158**, 275–282.

Petrelli, M., Perugini, D., Alagna, K. E., Poli, G. & Peccerillo, A., 2008. Spatially resolved and bulk trace element analysis by Laser Ablation-Inductively Coupled Plasma-Mass Spectrometry (LA-ICP-MS). *Periodico di Mineralogia*, **77**, 3–21.

Petrelli, M., Poli, G., Perugini, D. & Peccerillo, A., 2005. PetroGraph: a new software to visualize, model, and present geochemical data in igneous petrology. *Geochemistry Geophysics Geosystems*, **6**, Q07011, doi:10.1029/2005GC000932.

Philippot, P., Chevallier, P., Chopin, C. & Dubessy, J., 1995. Fluid composition and evolution in coesite-bearing rocks (Dora-Maira massif, Western Alps): implications for element recycling during subduction. *Contributions to Mineralogy and Petrology*, **121**, 29–44.

Pouchou, J. L. & Pichoir, F., 1988. Determination of mass absorption coefficients for soft X-Rays by use of the electron microprobe. *Microbeam Analysis*, San Francisco Press, 319–324.

Rudnick, R. L. & Gao, S., 2005. Composition of the continental crust. In: *The Crust* (Rudnick, R.L. ed), **3**, 1–64. In: *Treatise on geochemistry* (Holland, H.D. & Turekian, K.K. eds), Elsevier-Pergamon, Oxford, U.K..

Scambelluri, M., Bottazzi, P., Trommsdorff, V., Vannucci, R., Hermann, J., Gomez–Pugnaire, M. T. & Lòpez–Sànchez Vizcaìno, V., 2001. Incompatible element-rich fluids released by antigorite breakdown in deeply subducted mantle. *Earth and Planetary Science Letters*, **192**, 457–470.

Schertl, H.-P: & Schreyer, W., 2008. Geochemistry of coesite-bearing "pyrope quartzite" and related rocks from the Dora-Maira Massif, Western Alps. *European Journal of Mineralogy*, **20**, 791–809.

Schertl, H.-P., Schreyer, W. & Chopin, C., 1991. The pyrope-coesite rocks and their country rocks at Parigi, Dora Maira massif, western Alps: detailed petrography, mineral chemistry and PT-path. *Contributions to Mineralogy and Petrology,* **108,** 1–21.

Schmidt, M. W. & Poli, S., 1998. Experimentally based water budgets for dehydrating slabs and consequences for the arc magma generation. *Earth and Planetary Science Letters*, **163**, 361–379.

Schreyer, W., 1985. Metamorphism of crustal rocks at mantle depths: high-pressure minerals and mineral assemblages in metapelites. *Fortschritte der Mineralogie*, **63**, 227–261.

Sharp, Z. D. & Barnes, J. D., 2004. Water-soluble chlorides in massive seafloor serpentinites: a source of chloride in subduction zones. *Earth and Planetary Science Letters*, **226**, 243–254.

Sharp, Z. D., Essene, E. J. & Hunziker, J. C., 1993. Stable isotope geochemistry and phase equilibria of coesite-bearing whiteschists, Dora Maira Massif, western Alps. *Contributions to Mineralogy and Petrology*, **114,** 1–12.

Simon, G., Chopin, C. & Schenk, V., 1997. Near-end-member magnesiochloritoid in prograde-zoned pyrope, Dora-Maira massif, western Alps. *Lithos*, **41**, 37–57.

Tilton, G. R., Schreyer, W. & Schertl, H.-P., 1989. Pb-Sr-Nd isotopic behaviour of deeply subducted crustal rocks from the Dora Maira Massif, Western Alps, Italy. *Geochimica et Cosmochimica Acta*, **53**, 1391–1400.

Ulmer, P. & Trommsdorff, V., 1995. Serpentine stability to mantle depths and subduction-related magmatism. *Science*, **268**, 858–861.

USGS, 2009. Geochemical Reference Materials and Certificates. http://minerals.cr.usgs.gov/geo_chem_stand/

Vaggelli, G., Borghi, A., Cossio, R., Fedi, M., Giuntini, L., Lombardo, B., Marino, A., Massi, M., Olmi, F. & Petrelli M., 2006. Micro-PIXE analysis of monazite from the Dora Maira Massif , Western Italian Alps. *Microchimica Acta*, **155**, 305–311.

van Achterbergh, E., Ryan, C. G., Jackson, S. & Griffin, W. L., 2001. Data reduction software for LA-ICP-MS. In: *Laser-Ablation-ICPMS in the Earth sciences: principles and applications* (Sylvester, P. ed). *Mineralogical Association of Canada*, Short Course Series, **29**, 239–243.

Zack, T. & John, T., 2007. An evaluation of reactive fluid flow and trace element mobility in subducting slabs. *Chemical Geology*, **239**, 199–216.

FIGURE AND TABLE CAPTIONS

Fig. 1. (a) Simplified tectonic sketch-map of the Southern Dora-Maira Massif (modified from Castelli *et al*., 2007). Tectonic Units of the Massif are structurally listed from the lowest Pinerolo Unit to the highest Dronero-Sampeyre Unit. The inset shows the location of the Southern Dora-Maira Massif within a simplified tectonic sketch-map of the Western Alps. **Helvetic-Dauphinois domain**: MB = Mont Blanc-Aiguilles-Rouges. **Penninic domain**: SB = Grand St. Bernard Zone; MR = Monte Rosa; GP = Gran Paradiso; DM = Dora-Maira; V = Valosio; PZ = Piemonte zone of calcschists with meta-ophiolites. **Austroalpine Domain**: DB = Dent Blanche nappe; ME = Monte Emilius klippe; SZ = Sesia-Lanzo zone. SA = **Southern Alps**; EU = **Embrunais-Ubaye flysch nappe**; PF = Penninic thrust front; CL = Canavese line. (b) Simplified geological map of the coesite-bearing Brossasco-Isasca Unit (BIU) (modified from Castelli *et al*., 2007). Undifferentiated units: graphite-rich schists and metaclastics of the epidote-blueschist facies “Pinerolo Unit”; “San Chiaffredo Unit” and “Rocca Solei Unit” with pre-Alpine basement rocks overprinted by Alpine quartz-eclogite facies metamorphism. The white stars show the two locations of the studied whiteschists.

Fig. 2. Simplified sketch showing the three types of pyropes recognised in the studied UHP whiteschists and their chemical zoning: megablast (a), porphyroblast (b), neoblast (c).

Fig. 3. (a) Chemical compositions of garnet in the (grossular + andradite + spessartine) – pyrope – almandine diagram. The pyrope component increases from prograde Prp I to peak Prp II and decreases to Prp III. (b) Chemical compositions of white mica in the Si (a.p.f.u.) vs. ($Mg + Fe^{2+}$) diagram. Prograde white mica is a muscovite, whereas peak and retrograde white micas are phengites with decreasing Si contents.

Fig. 4. Trace-element pattern of UHP whiteschists and metagranite normalised to primordial mantle (PM) from McDonough and Sun (1995). For comparison, the trace-element composition of the average continental crust from Rudnick & Gao (2005) is also reported. With respect to the metagranite, the whiteschists are enriched in HREE, Y and, locally, Hf and Zr, and they are depleted in Cs, Pb, Rb, Sr, Ba, and Eu.

Fig. 5. Trace-element concentrations in Prp II (a), white mica (b), dumortierite and ellenbergerite (c) from UHP whiteschists. Trace-element concentrations are normalised to primordial mantle (McDonough & Sun, 1995). Data below detection limits, that are not represented by symbols and connected with dashed lines, are plotted as detection limit values. The diagrams show that garnet and ellenbergerite preferentially partition HREE and Y, ellenbergerite and dumortierite partition HFSE (Zr, Hf, Ti, Ta, Nb), and white micas partition LILE (K, Rb, Cs, Ba, Pb).

Fig. 6. Photomicrographs of fluid and MS inclusions within UHP whiteschists. (a) Primary three-phase (S + L + V) inclusion elongated parallel to the c-axis of the host prograde Ky I. Sample DM1598; Plane Polarised Light (PPL). (b) Primary MS inclusions marking the growth zones in the UHP peak Prp II. Sample DM1616, PPL. (c) A preserved MS inclusion, characterised by negative crystal shape, occurs together with re-equilibrated inclusions, surrounded by haloes of very tiny fluid inclusions. Sample DM1598; PPL. (d) Preserved MS inclusion containing the typical mineral assemblage Mg-chlorite, Na-K phlogopite, Zn-rich pyrite, and Cl-rich apatite. Sample DM1035; crossed polarizer. (e) Back-scattered electron (BSE) image of a freshly-broken surface of a pyrope including a MS inclusion. Note the intimate intergrowth between Mg-chlorite and Na-phlogopite,

suggesting equilibrium co-precipitation. Sample DM69. (f) BSE image of a MS inclusion containing a large incidentally-trapped rutile. Sample DM69.

Fig. 7. Trace-element concentrations in MS inclusions + Prp II normalised to the primordial mantle (McDonough & Sun, 1995), compared with those in Prp II (from Fig. 6a), Phg I (from Fig. 6b), and whole-rock (from Fig. 5). The fluid within MS inclusion is enriched in LILE (Pb, Cs, Sr, Rb, K, LREE, Ba), Th, and U. Its pattern is consistent with the crustal signature of the UHP whiteschists and, if compared with Prp II and Phg I, reveals achievement of fluid-rock chemical equilibrium during UHP metamorphism.

Fig. 8. Metamorphic evolution of the UHP whiteschists from BIU based on present and previously published data (e.g., Chopin (1984; 1986); Schreyer (1985), Chopin *et al*. (1986; 1991), Schreyer *et al*. (1991), Compagnoni *et al*. (1995), Chopin & Schertl (1999), Hermann (2003). Minerals observed in the studied samples are in italics.

Fig. 9. *P-T* diagram showing the *P-T* path of the UHP whiteschists from BIU. The reaction curve Ky + Chl + Tlc = Grt + fluid (in black), the wet granite *solidus* (thick curve in grey), and the curves representing the % of H_2O in the liquid phase (dashed-dotted curves in grey) are from Hermann (2003). The grey dot is the second critical end-point for the granitic system. The three black dashed curves of antigorite breakdown to give Ol + Opx + fluid at different a_{H2O} are from Sharp & Barnes (2004). The black dashed-dotted line is the experimental curve of the antigorite breakdown (a_{H2O} = 1) from Ulmer & Trommsdorff (1995). The black dotted line is the curve for antigorite breakdown (a_{H2O} = 1) from Schmidt & Poli (1998).

Fig. 10. Origin and evolution, up to UHP peak, of the UHP whiteschists from BIU. The different generations of garnets are shown (cf. Fig. 2). An original post-Variscan granitoid, including a xenolith of the country Variscan metamorphic basement, undergoes an Alpine prograde HP to UHP metamorphism. At stage A, an almandine-rich garnet grows in the xenolith. Subsequently (stages B and C), the infiltration along shear zones of high-salinity, high-Mg fluids, generated from dehydration of antigorite in subducting serpentinites, metasomatised the orthogneiss and the xenoliths to generate the whiteschists. At the same time, metamorphic dehydration reactions—involving talc, muscovite, and Mg-chlorite—also occurred within the whiteschists. At stage D, the peak mineral assemblage that formed in the presence of an alumino-silicate, supercritical liquid enriched in LILE, Th, and U likely originated by dehydration reactions involving talc and phlogopite. See text for further explanation.

Table 1. Representative chemical analyses of different generations of garnet and white mica from UHP whiteschists

Table 2. Major- (wt% Oxide) and trace- (ppm) element compositions of UHP whiteschists and UHP metagranite; in brackets, the wt% values calculated on anhydrous basis; mg# = $Mg/(Mg+Fe_{tot})$

Table 3. Representative trace-element concentrations (ppm) of garnet, white mica, Mg-dumortierite and ellenbergerite from UHP whiteschists. * = spot analysis of 60 μm

Table 4. Representative trace-element concentrations (ppm) of MS inclusions within peak Prp II (see table 3)

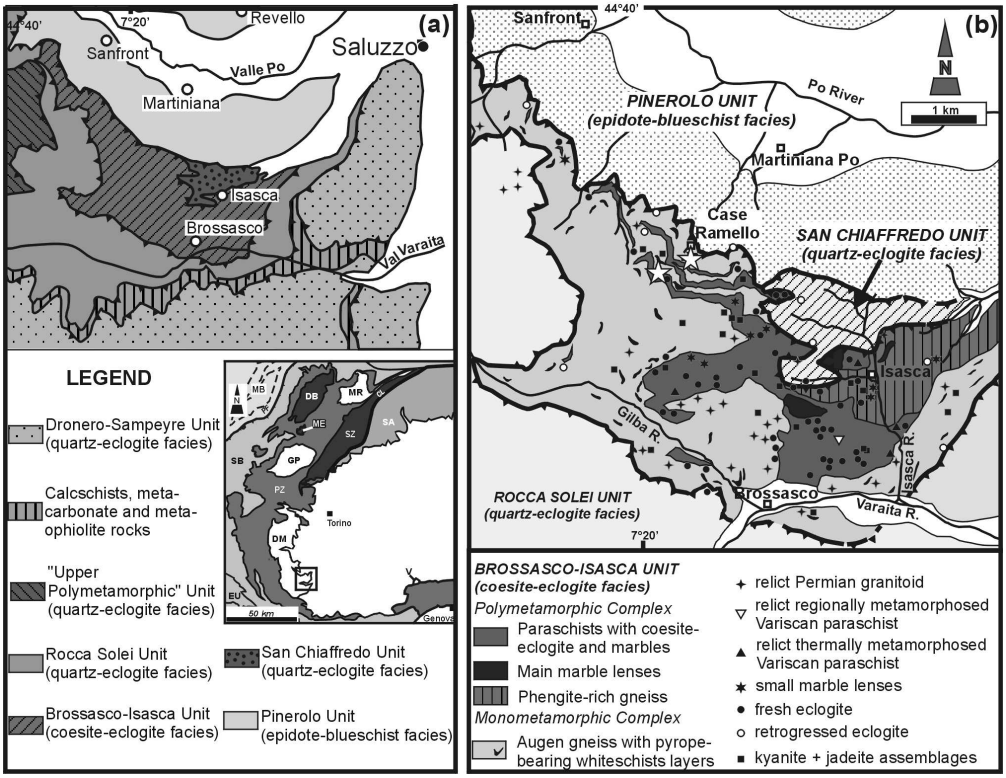
(a)
Revello
Saluzzo
Sanfront
Valle Po
Martiniana
Isasca
Brossasco
Val Varaita
7°20'
44°40'
LEGEND
Dronero-Sampeyre Unit (quartz-eclogite facies)
Calcschists, meta-carbonate and meta-ophiolite rocks
"Upper Polymetamorphic" Unit (quartz-eclogite facies)
Rocca Solei Unit (quartz-eclogite facies)
San Chiaffredo Unit (quartz-eclogite facies)
Brossasco-Isasca Unit (coesite-eclogite facies)
Pinerolo Unit (epidote-blueschist facies)
MB
DB
MR
ME
SZ
SA
SB
GP
PZ
DM
EU
Torino
50 km
Genova
(b)
Sanfront
44°40'
N
Po River
1 km
PINEROLO UNIT
(epidote-blueschist facies)
Martiniana Po
Case Ramello
SAN CHIAFFREDO UNIT
(quartz-eclogite facies)
Isasca
Gilba R.
Isasca R.
ROCCA SOLEI UNIT
(quartz-eclogite facies)
Brossasco
Varaita R.
7°20'
BROSSASCO-ISASCA UNIT
(coesite-eclogite facies)
Polymetamorphic Complex
Paraschists with coesite-eclogite and marbles
Main marble lenses
Phengite-rich gneiss
Monometamorphic Complex
Augen gneiss with pyrope-bearing whiteschists layers
relict Permian granitoid
relict regionally metamorphosed Variscan paraschist
relict thermally metamorphosed Variscan paraschist
small marble lenses
fresh eclogite
retrogressed eclogite
kyanite + jadeite assemblages

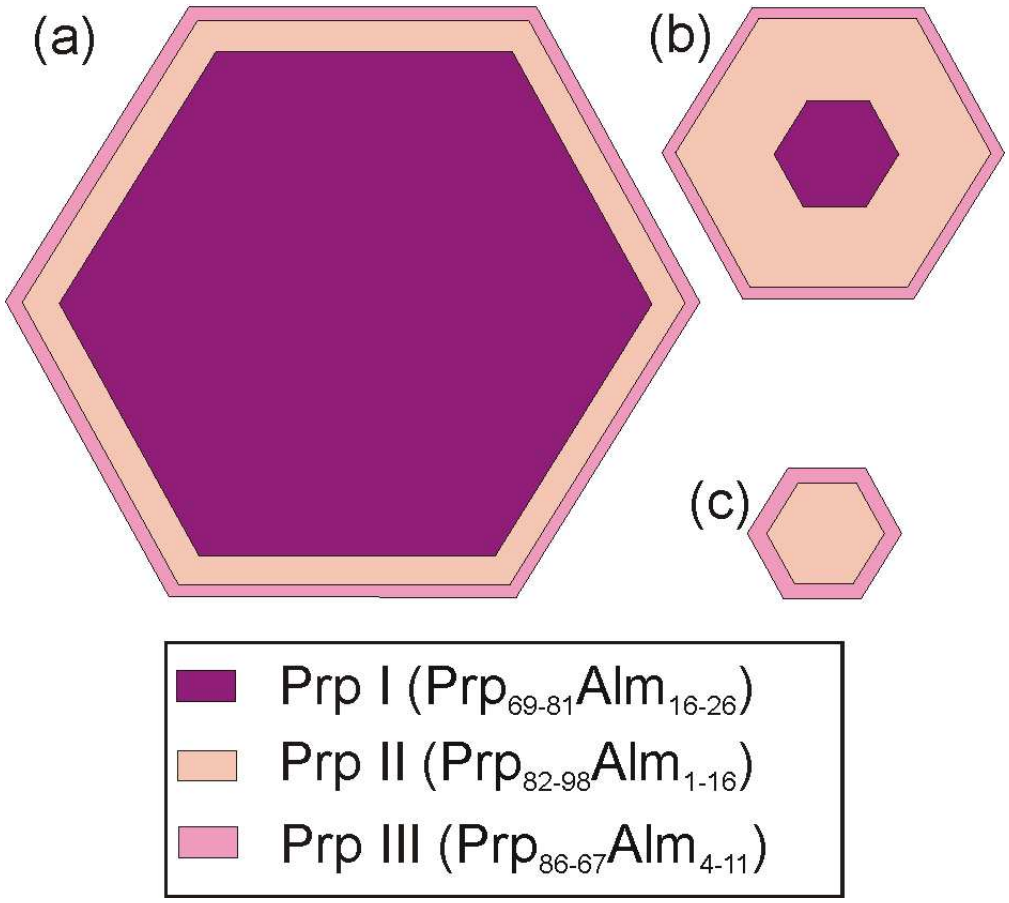
(a)
(b)
(c)
Prp I (Prp69-81Alm16-26)
Prp II (Prp82-98Alm1-16)
Prp III (Prp86-67Alm4-11)

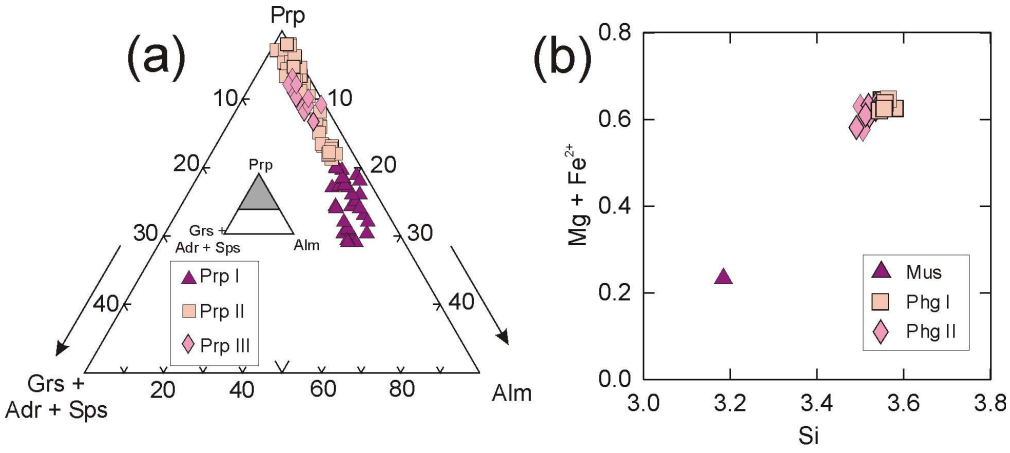
(a)
Prp
10
20
30
40
Grs +
Adr + Sps
20
40
60
80
Alm
Prp
Grs +
Adr + Sps
Alm
Prp I
Prp II
Prp III
(b)
0.8
0.6
0.4
0.2
0.0
Mg + Fe2+
3.0
3.2
3.4
3.6
3.8
Si
Mus
Phg I
Phg II

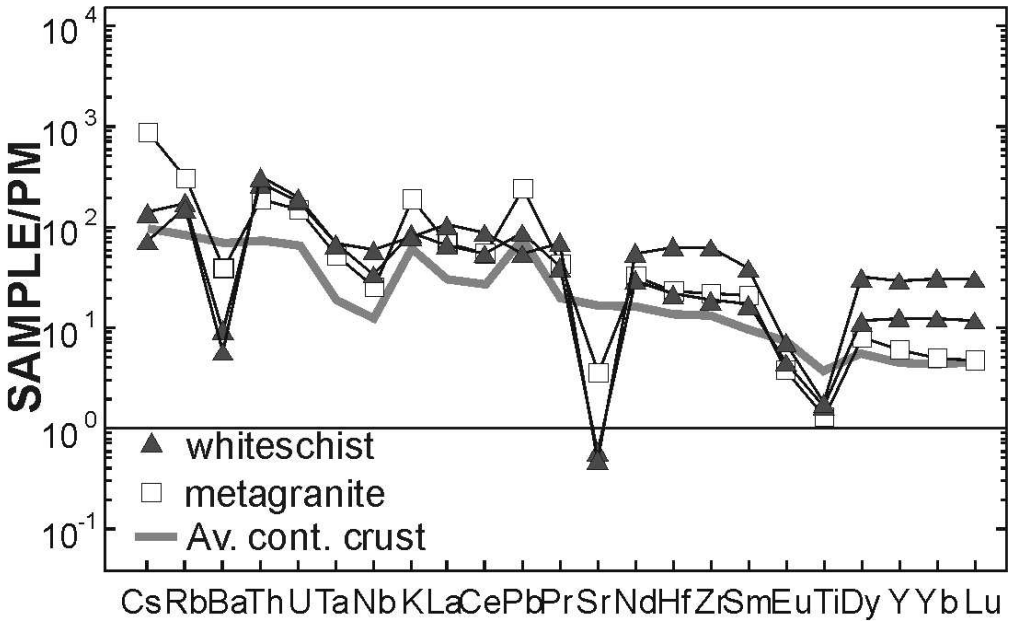
SAMPLE/PM
10^4
10^3
10^2
10^1
10^0
10^-1
whiteschist
metagranite
Av. cont. crust
Cs Rb Ba Th U Ta Nb K La Ce Pb Pr Sr Nd Hf Zr Sm Eu Ti Dy Y Yb Lu

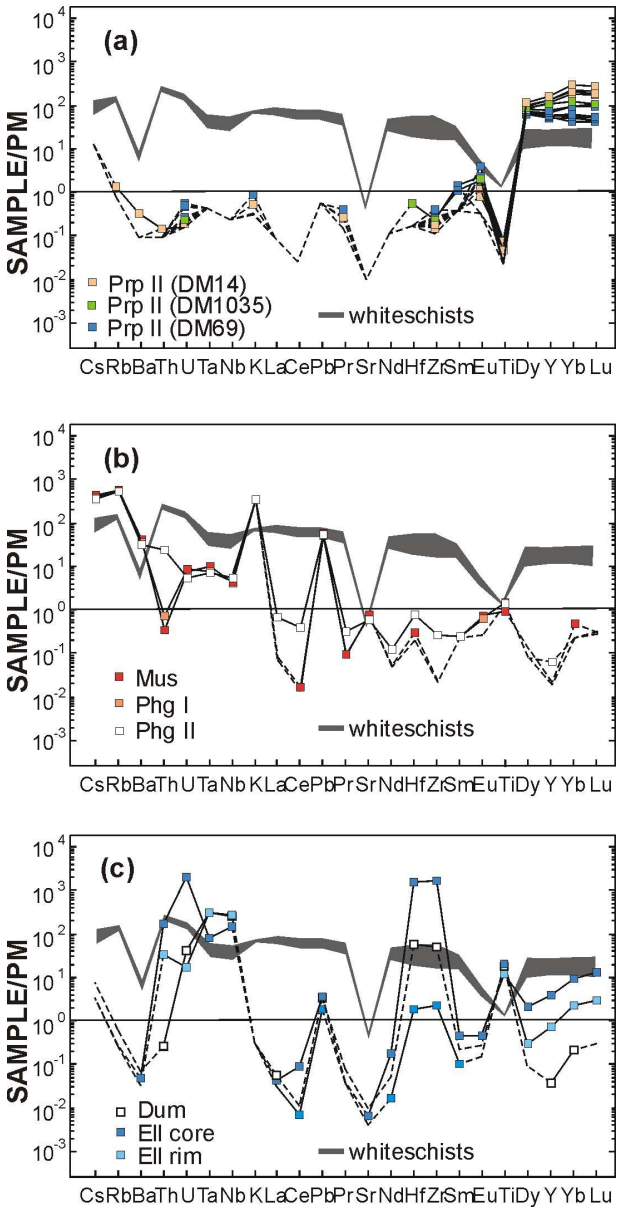
(a)
SAMPLE/PM
Prp II (DM14)
Prp II (DM1035)
Prp II (DM69)
whiteschists
CsRbBaThUTaNbKLaCePbPrSrNdHfZrSmEuTiDyYYbLu
(b)
SAMPLE/PM
Mus
Phg I
Phg II
whiteschists
CsRbBaThUTaNbKLaCePbPrSrNdHfZrSmEuTiDyYYbLu
(c)
SAMPLE/PM
Dum
Ell core
Ell rim
whiteschists
CsRbBaThUTaNbKLaCePbPrSrNdHfZrSmEuTiDyYYbLu

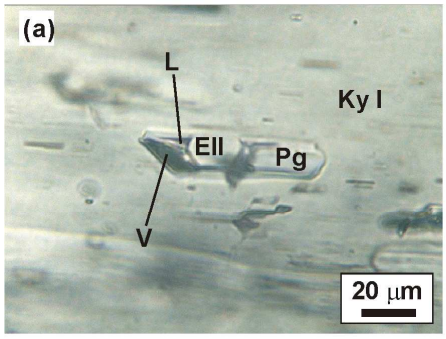
(a)
L
Ky I
Ell
Pg
V
20 μm

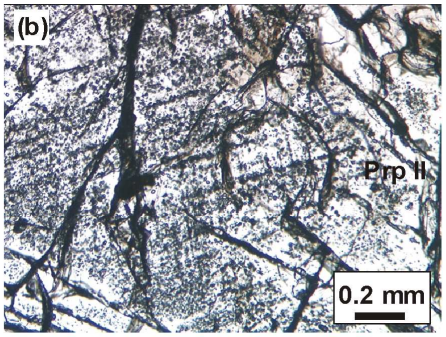
(b)
Prp II
0.2 mm

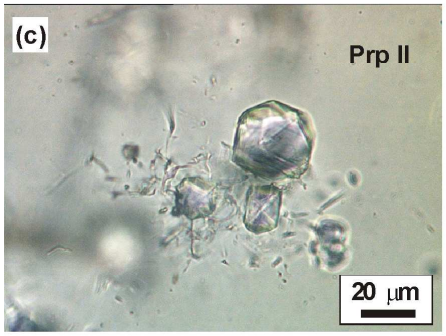
(c)
Prp II
20 μm

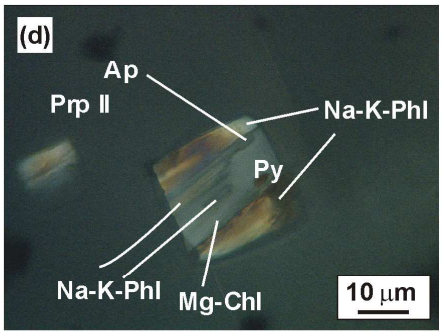
(d)
Ap
Prp II
Na-K-Phl
Py
Na-K-Phl
Mg-Chl
10 μm

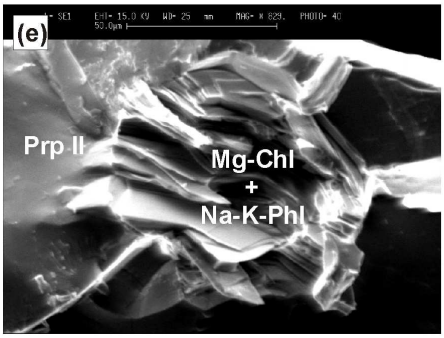
(e)
Prp II
Mg-Chl
+
Na-K-Phl

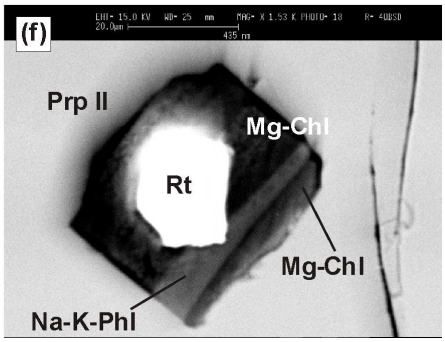
(f)
Prp II
Mg-Chl
Rt
Mg-Chl
Na-K-Phl

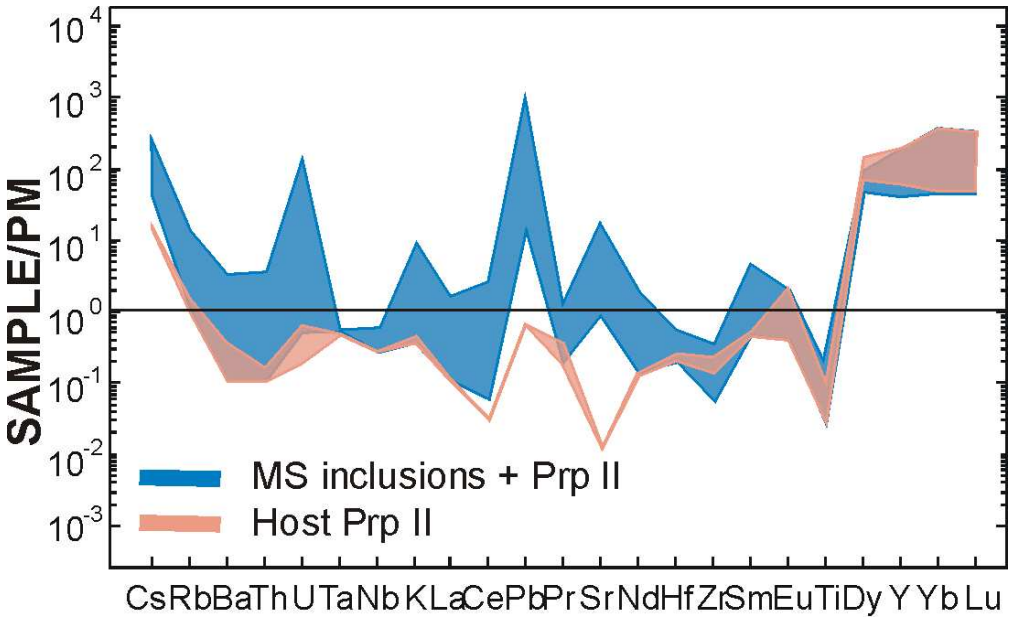
SAMPLE/PM
10^4
10^3
10^2
10^1
10^0
10^-1
10^-2
10^-3
MS inclusions + Prp II
Host Prp II
Cs Rb Ba Th U Ta Nb K La Ce Pb Pr Sr Nd Hf Zr Sm Eu Ti Dy Y Yb Lu

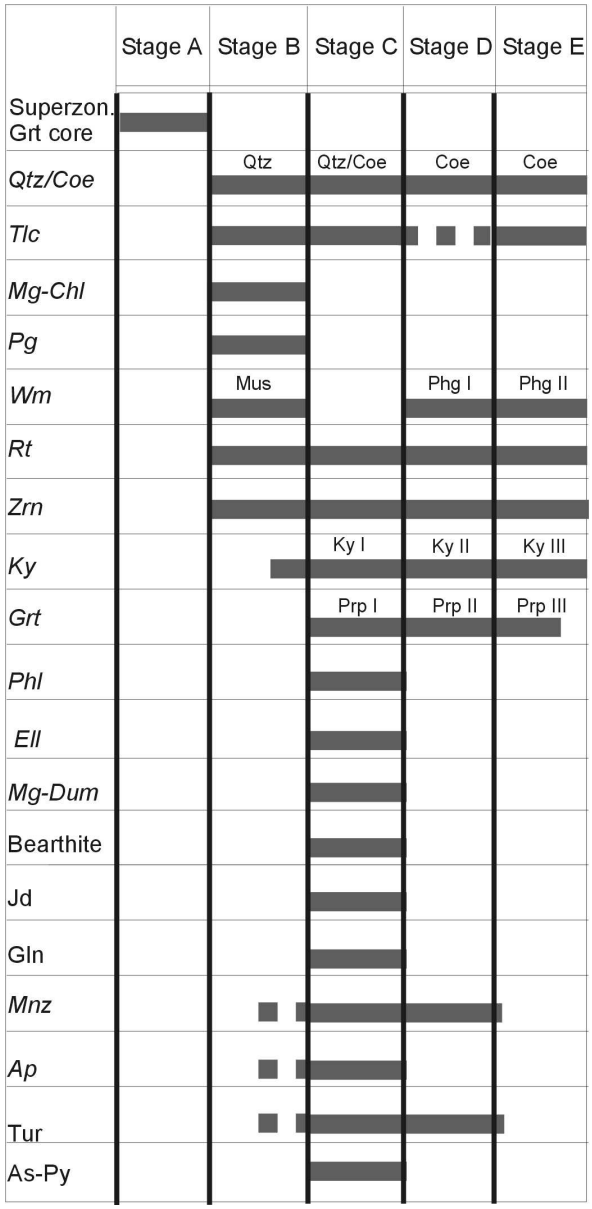
Stage A
Stage B
Stage C
Stage D
Stage E
Superzon. Grt core
Qtz/Coe
Qtz
Qtz/Coe
Coe
Coe
Tlc
Mg-Chl
Pg
Wm
Mus
Phg I
Phg II
Rt
Zrn
Ky
Ky I
Ky II
Ky III
Grt
Prp I
Prp II
Prp III
Phl
Ell
Mg-Dum
Bearthite
Jd
Gln
Mnz
Ap
Tur
As-Py

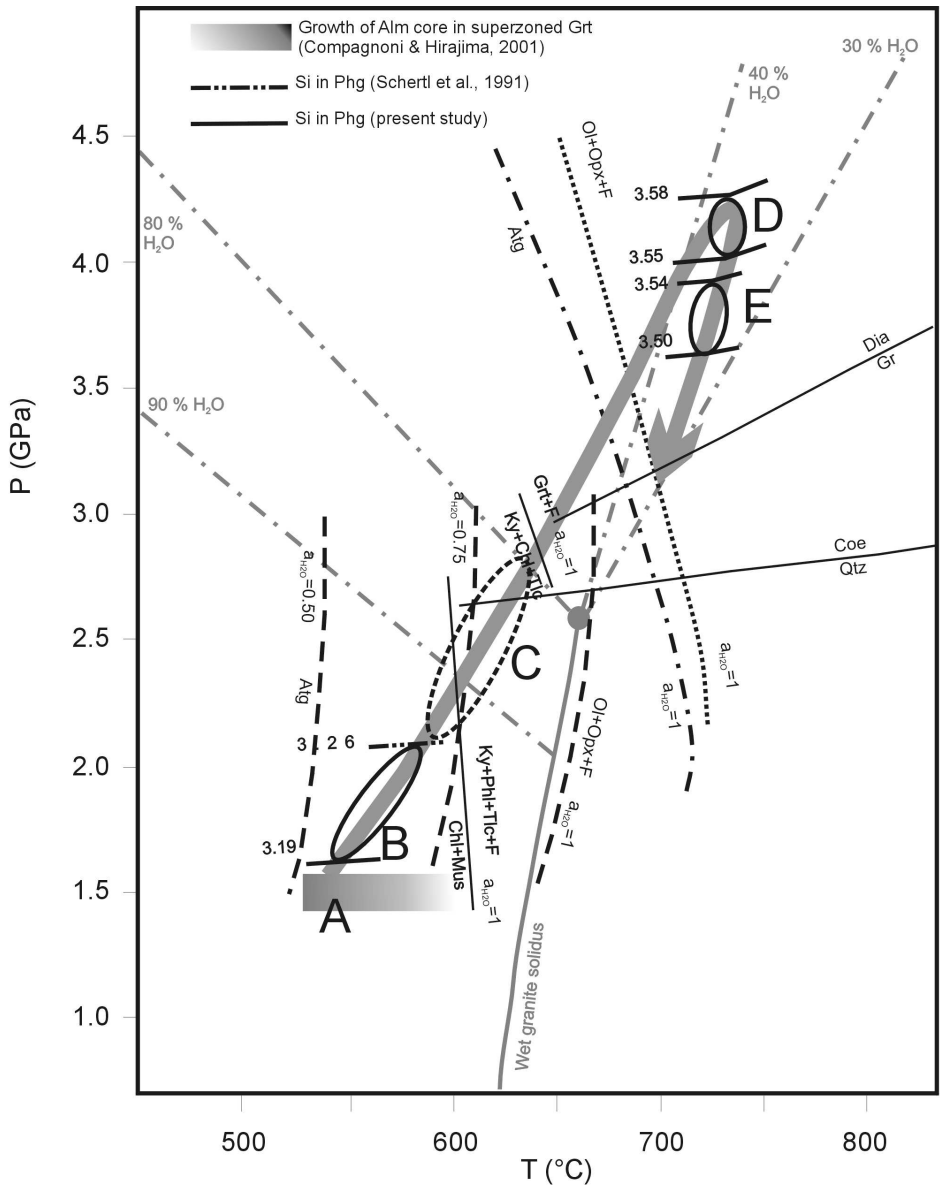
Growth of Alm core in superzoned Grt
(Compagnoni & Hirajima, 2001)
Si in Phg (Schertl et al., 1991)
Si in Phg (present study)
30 % H2O
40 % H2O
80 % H2O
90 % H2O
Ol+Opx+F
Atg
3.58
3.55
3.54
3.50
D
E
Dia
Gr
Coe
Qtz
Grt+F
Ky+Chl+Tlc
aH2O=0.75
aH2O=0.50
aH2O=1
C
Atg
3 2 6
3.19
B
A
Ky+Phl+Tlc+F
Chl+Mus
Wet granite solidus
P (GPa)
T (°C)
4.5
4.0
3.5
3.0
2.5
2.0
1.5
1.0
500
600
700
800

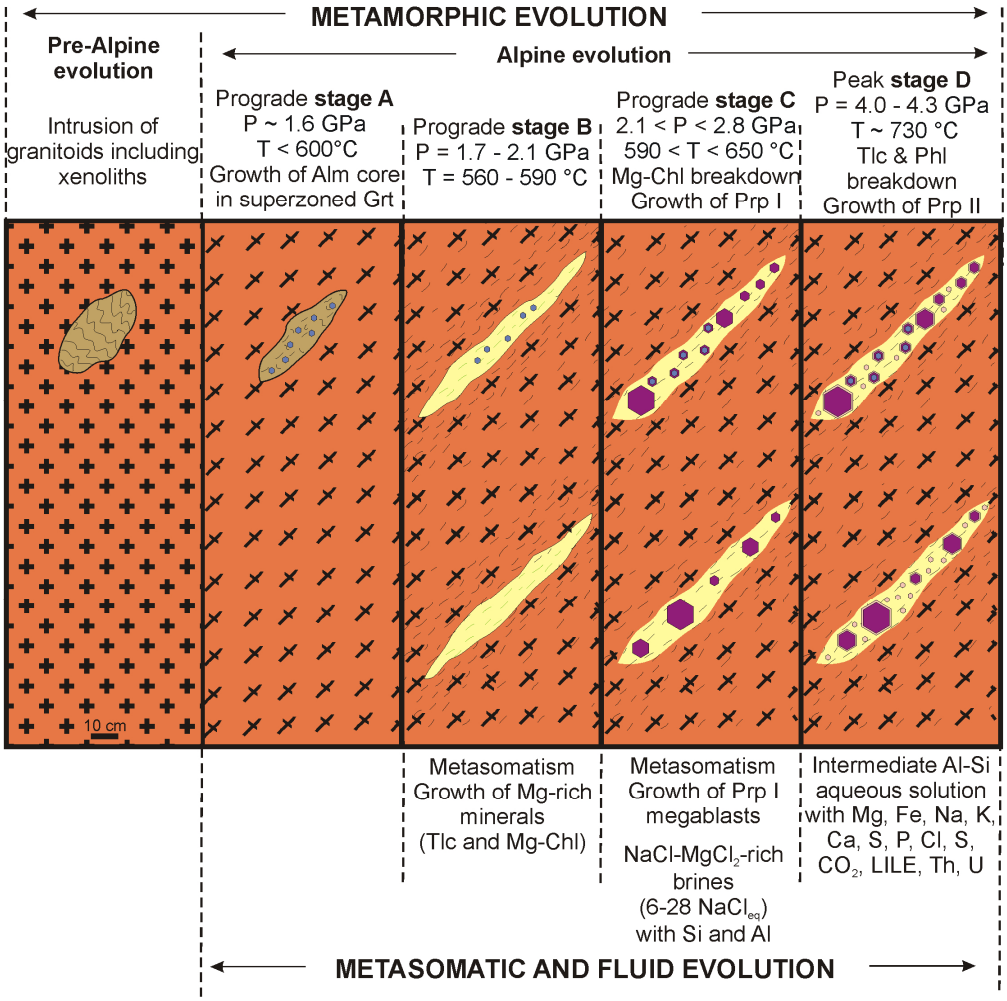
METAMORPHIC EVOLUTION
Pre-Alpine evolution
Intrusion of granitoids including xenoliths
Alpine evolution
Prograde stage A
P ~ 1.6 GPa
T < 600°C
Growth of Alm core in superzoned Grt
Prograde stage B
P = 1.7 - 2.1 GPa
T = 560 - 590 °C
Prograde stage C
2.1 < P < 2.8 GPa
590 < T < 650 °C
Mg-Chl breakdown
Growth of Prp I
Peak stage D
P = 4.0 - 4.3 GPa
T ~ 730 °C
Tlc & Phl breakdown
Growth of Prp II
10 cm
Metasomatism
Growth of Mg-rich minerals
(Tlc and Mg-Chl)
Metasomatism
Growth of Prp I megablasts
NaCl-MgCl2-rich brines
(6-28 NaCleq)
with Si and Al
Intermediate Al-Si aqueous solution with Mg, Fe, Na, K, Ca, S, P, Cl, S, CO2, LILE, Th, U
METASOMATIC AND FLUID EVOLUTION

	DM14	DM69	DM69	DM1035	DM1597	DM1605	DM1598	DM1598	DM1596	DM1596	DM1598	DM1596	DM1597	DM1598
	14_8Grt103	69_20Grt122	9_15Grt12	24Grt128	34Grt191	1605Grt194	25Grt159	24Wm149	6Wm168	6Wm172	23Wm130	6Wm170	33AWm185	23Wm136
	Prp I	Prp I	Prp I	Prp II	Prp II	Prp II	Prp III	Muscovite	Phg I	Phg I	Phg I	Phg II	Phg II	Phg II
wt%														
SiO_2	41.82	42.24	42.28	42.82	44.23	44.59	43.17	47.28	54.02	53.81	53.59	53.28	53.54	52.26
P_2O_5	--	0.06	0.11	0.12	0.20	0.17	0.20	0.05	0.01	--	0.01	0.03	0.03	--
TiO_2	--	--	0.04	0.05	0.04	--	0.08	0.27	0.30	0.34	0.33	0.38	0.21	0.21
ZrO_2	0.09	--	0.13	0.10	0.02	--	--	--	--	--	0.01	--	0.10	--
Al_2O_3	24.51	24.90	25.19	25.08	25.61	26.00	25.18	32.14	23.97	23.88	23.08	24.94	23.74	24.12
Cr_2O_3	0.00	0.03	0.01	--	--	0.02	--	--	0.01	0.01	--	0.04	--	0.03
FeO	11.92	9.93	8.25	7.94	1.98	1.06	5.50	0.35	0.34	0.26	0.15	0.24	0.19	0.18
MnO	0.84	0.10	0.13	0.21	0.02	--	0.06	--	--	0.02	0.02	0.02	--	0.02
MgO	19.61	22.21	23.10	24.02	27.89	28.50	24.47	2.15	6.16	6.17	6.21	5.82	6.23	6.23
CaO	1.83	1.19	1.02	1.01	0.10	0.16	1.03	0.01	--	--	0.01	--	0.01	--
Na_2O	0.05	0.06	0.04	0.06	0.07	0.06	0.07	2.70	0.10	0.13	0.11	0.20	0.06	0.11
K_2O	0.01	--	0.01	0.00	--	0.02	--	8.20	10.01	10.39	10.25	10.55	10.88	11.06
F	0.08	--	--	0.07	--	0.04	0.10	0.05	0.35	0.19	0.07	0.36	0.25	0.08
Cl	--	0.02	0.01	--	--	--	0.01	0.02	0.01	--	--	--	0.02	--
SUM	100.68	100.72	100.31	101.41	100.16	100.58	99.76	93.14	94.93	95.01	93.78	95.50	94.98	94.22
O=F	0.034	0.000	0.000	0.029	0.000	0.017	0.042	0.021	0.146	0.078	0.030	0.151	0.105	0.035
O=Cl	0.000	0.005	0.002	0.000	0.000	0.000	0.002	0.004	0.002	0.000	0.000	0.000	0.004	0.000
TOT	100.65	100.71	100.31	101.38	100.16	100.57	99.72	93.110	94.779	94.936	93.752	95.348	94.873	94.182
CATIONS calculated on the basis of 12 oxygen								CATIONS calculated on the basis of 11 oxygen						
Si	2.968	2.956	2.948	2.949	2.988	2.986	2.980	3.185	3.550	3.548	3.580	3.495	3.540	3.500
Al	2.050	2.053	2.070	2.035	2.039	2.052	2.048	2.551	1.856	1.855	1.817	1.928	1.850	1.903
P	--	0.003	0.007	0.007	0.012	0.010	0.012	0.003	0.001	--	0.001	0.002	0.002	--
Ti	--	--	0.002	0.003	0.002	--	0.004	0.014	0.015	0.017	0.017	0.019	0.010	0.010
Zr	0.003	--	0.004	0.003	0.001	--	--	--	--	--	0.000	--	0.003	--
Cr	0.000	0.002	0.001	--	--	0.001	--	--	0.001	0.001	--	0.002	--	0.002
Fe^{2+}	0.707	0.581	0.481	0.457	0.112	0.059	0.317	0.020	0.019	0.015	0.008	0.013	0.010	0.010
Mn	0.050	0.006	0.008	0.012	0.001	--	0.004	--	--	0.001	0.001	0.001	--	0.001
Mg	2.073	2.315	2.400	2.464	2.807	2.843	2.516	0.216	0.603	0.606	0.618	0.569	0.614	0.621
Ca	0.139	0.089	0.076	0.074	0.007	0.011	0.076	0.001	--	--	0.001	--	0.001	--
Na	0.007	0.008	0.005	0.008	0.009	0.008	0.009	0.352	0.013	0.017	0.014	0.025	0.008	0.014
K	0.001	--	0.001	0.000	--	0.002	--	0.704	0.839	0.874	0.873	0.882	0.917	0.945
F	0.009	--	--	0.008	--	0.004	0.011	0.005	0.036	0.019	0.007	0.037	0.026	0.009
Cl	--	0.001	0.001	--	--	--	0.001	0.001	0.000	--	--	--	0.001	--
Al^{IV}	0.032	0.040	0.045	0.044	--	0.004	0.008	0.812	0.450	0.452	0.420	0.504	0.459	0.499
Al^{VI}	2.018	2.013	2.025	1.991	2.038	2.048	2.040	1.738	1.406	1.403	1.397	1.424	1.391	1.404
ENDMEMBERS														
Alm	0.238	0.194	0.162	0.152	0.038	0.020	0.109							
Prp	0.698	0.774	0.809	0.819	0.959	0.976	0.864							
Sps	0.017	0.002	0.003	0.004	0.000	0.000	0.001							

Ca-Grt	0.047	0.030	0.026	0.025	0.002	0.004	0.026

	DM69	DM1035	DM989
	whiteschist	whiteschist	metagranite
wt%			
SiO_2	71.9 (73.30)	66.7 (70.77)	73.22 (74.48)
TiO_2	0.33 (0.34)	0.35 (0.37)	0.25 (0.25)
Al_2O_3	14.5 (14.78)	14.65 (15.54)	13.50 (13.73)
Fe_2O_3	0.20	0.02	0.66
FeO	1.21	1.77	1.42
FeO_{TOT}	1.39 (1.42)	1.78 (1.89)	2.02 (2.05)
MnO	0.01 (0.01)	0.02 (0.02)	0.05 (0.05)
MgO	5.54 (5.65)	6.77 (7.18)	0.33 (0.34)
CaO	0.19 (0.19)	0.16 (0.17)	0.90 (0.92)
Na_2O	0.09 (0.09)	0.09 (0.10)	2.74 (2.79)
K_2O	2.46 (2.52)	2.27 (2.41)	5.18 (5.27)
P_2O_5	<0.01	0.07 (0.07)	0.12 (0.12)
LOI	1.66	1.38	0.74
TOT	98.09	94.25	99.11
mg#	0.80	0.79	0.19
ppm			
V	16	8.0	34
Cr	10	10	30
Co	1.8	1.5	6.5
Cu	7.0	15	6.0
Zn	22	40	70
Rb	103	91	178
Sr	11	9	68
Y	53	124	25
Zr	194	651	228
Nb	22	39	16
Cs	2.9	1.5	18
Ba	61	37	255
La	43	66	45
Ce	89	146	89
Pr	10	17	11
Nd	37	68	39
Sm	7	15	8
Eu	0.68	1.1	0.6
Gd	5.9	16	7.3
Tb	1.1	3.2	1.0
Dy	7.6	21	5.2
Ho	1.8	4.9	0.91
Er	5.5	14	2.4
Tm	0.85	2.1	0.35
Yb	5.3	13	2.1
Lu	0.78	2.1	0.32
Hf	6.0	18	6.4
Ta	2.5	2.5	1.9
Pb	13	8.0	35
Th	21	25	15
U	3.7	3.9	3.0
Ga	16	21	31
Mo	<2	<2	<2
Ni	<5	<5	7.0
Sn	7.0	7.0	11
Tl	<0.5	<0.5	<0.5
W	3.0	3.0	2.0
Ag	<1	<1	<1

	DM69	DM14	DM1597	DM1597	DM1597	DM1605	DM1605*	DM1605*
	Grt_of_MSI8	Grt_of_MSI13	05_Phe_core	06_Phe_rim	07_WM_1	05_Dum	06_Ellemb_1rim	07_Ellemb_2core
	Prp II	Prp II	Phg I	Phg II	Muscovite	Mg-Dumortierite	Ellembergerite	Ellembergerite
ppm								
V	<0.5	7.7	44	48	48	55	47	34
Cr	<2	<2	<2	26	8.0	<2	13	5.5
Co	<1	5.7	<1	<1	<1	<1	1.2	0.91
Cu	<2	<2	<2	<2	<2	<2	1.3	1.5
Zn	45	16	<1	<1	6.6	8.1	38	40
Rb	<0.5	0.91	366	358	343	<0.5	<0.08	<0.08
Sr	<0.1	<0.1	15	16	12	<0.1	<0.06	0.15
Y	360	529	<0.1	<0.1	0.30	0.19	3.6	19
Zr	2.7	2.0	<0.4	<0.4	3.1	599	28	19970
Nb	<0.1	<0.1	2.9	3.1	3.8	184	197	112
Cs	<0.2	<0.2	9.6	8.3	7.8	<0.2	<0.06	<0.06
Ba	<0.4	2.5	279	243	225	<0.4	<0.1	0.38
La	<0.05	<0.05	<0.05	<0.05	0.48	0.04	<0.02	0.03
Ce	<0.05	<0.05	0.03	<0.05	0.72	<0.05	0.01	0.18
Pr	0.11	<0.04	<0.04	0.02	0.09	<0.04	<0.04	<0.04
Nd	<0.1	<0.1	<0.1	<0.1	0.17	<0.1	0.02	0.25
Sm	0.63	<0.1	<0.1	<0.1	0.11	<0.1	0.05	0.20
Eu	<0.05	0.14	0.12	0.10	<0.05	<0.05	<0.02	0.08
Gd	7.6	5.2	<0.2	<0.2	<0.2	<0.2	0.17	0.56
Tb	4.7	4.6	<0.02	<0.02	<0.02	<0.02	0.02	0.22
Dy	48	61	<0.06	<0.06	<0.06	<0.06	0.23	1.7
Ho	10	21	0.03	<0.01	<0.01	0.02	0.10	0.53
Er	28	71	<0.04	<0.04	0.07	<0.04	0.5	2.2
Tm	3.7	12	<0.02	<0.02	<0.02	<0.02	0.09	0.52
Yb	31	92	0.23	<0.01	<0.01	0.11	1.2	4.7
Lu	4.1	13	<0.02	<0.02	<0.02	<0.02	0.24	1.01
Hf	<0.05	<0.05	0.09	<0.05	0.23	19	0.603	490.38
Ta	<0.02	<0.02	0.38	0.30	0.28	13	13	3.4
Pb	<0.1	<0.1	8.2	9.2	8.6	0.57	0.32	0.62
Th	<0.008	<0.008	0.03	0.06	2.0	0.02	3.0	15
U	0.006	<0.004	0.17	0.19	0.11	0.96	0.40	46
K	250	<50	83000	82000	83000	<50	<10	<10
Ti	<10	102	1140	1860	1671	23800	27600	16100

	DM69 MSI4	DM69 MSI5	DM14 MSI13	DM14 MSI13b	DM14 MSI19b	DM14 MSI43
ppm						
V	<0.5	<0.5	7.2	9.0	<0.5	<0.5
Cr	<2	<2	<2	<2	<2	<2
Co	<1.5	<1.5	9.4	3.4	<1.5	<1.5
Cu	<2	<2	<2	<2	<2	<2
Zn	157	110	19	161	276	35
Rb	6.7	<0.5	4.0	7.7	<0.5	5.6
Sr	124	25	29	240	321	51
Y	180	203	457	520	260	692
Zr	<0.4	<0.4	1.31	3.8	<0.5	<0.5
Nb	<0.1	0.42	<0.1	<0.1	<0.1	<0.1
Cs	5.3	2.0	3.0	3.9	3.8	5.3
Ba	21	4.1	5.6	19	8.0	<0.4
La	0.98	0.29	0.23	0.42	0.68	<0.05
Ce	4.0	0.44	0.26	1.6	1.5	0.42
Pr	0.31	<0.04	0.10	0.24	<0.04	<0.04
Nd	1.7	<0.1	0.58	2.5	0.76	<0.1
Sm	0.63	<0.1	<0.1	1.9	1.3	0.75
Eu	<0.05	0.19	<0.05	0.31	<0.05	<0.05
Gd	4.5	4.5	5.3	8.6	3.0	7.3
Tb	2.9	3.7	4.0	4.5	2.1	4.9
Dy	30	34	57	60	30	66
Ho	6.9	8.3	19	20	9.8	24
Er	19	19	62	70	31	91
Tm	2.7	3.2	11	13	4.9	17
Yb	21	20	82	90	41	133
Lu	3.3	2.9	12	13	4.9	18
Hf	0.11	<0.05	0.15	<0.05	<0.05	<0.05
Ta	<0.02	<0.02	<0.02	<0.02	<0.02	<0.02
Pb	17	13	84	138	8	2
Th	0.13	0.05	<0.008	0.31	<0.008	0.02
U	0.39	0.01	0.02	2.4	0.12	0.15
K	1744	328	759	1397	529	442
Ti	237	164	90	111	140	46